CRITICAL REVIEWS IN BIOTECHNOLOGY
2018, VOL. 38, NO. 7, 1003–1024
https://doi.org/10.1080/07388551.2018.1426555

Taylor & Francis
Taylor & Francis Group

REVIEW ARTICLE



# Various physicochemical and surface properties controlling the bioactivity of cerium oxide nanoparticles

Bing-Huei Chen[a,b] and Baskaran Stephen Inbaraj[a]

[a]Department of Food Science, Fu Jen Catholic University, New Taipei City, Taiwan; [b]Graduate Institute of Medicine, Fu Jen Catholic University, New Taipei City, Taiwan

**ABSTRACT**

Amidst numerous emerging nanoparticles, cerium oxide nanoparticles (CNPs) possess fascinating pharmacological potential as they can be used as a therapeutic for various oxidative stress-associated chronic diseases such as cancer, inflammation and neurodegeneration due to unique redox cycling between $Ce^{3+}$ and $Ce^{4+}$ oxidation states on their surface. Lattice defects generated by the formation of $Ce^{3+}$ ions and compensation by oxygen vacancies on CNPs surface has led to switching between $CeO_2$ and $CeO_{2-x}$ during redox reactions making CNPs a lucrative catalytic nanoparticle capable of mimicking key natural antioxidant enzymes such as superoxide dismutase and catalase. Eventually, most of the reactive oxygen species and nitrogen species in biological system are scavenged by CNPs via an auto-regenerative mechanism in which a minimum dose can exhibit catalytic activity for a longer duration. Due to the controversial outcomes on CNPs toxicity, considerable attention has recently been drawn towards establishing relationships between the physicochemical properties of CNPs obtained by different synthesis methods and biological effects ranging from toxicity to therapeutics. Unlike non-redox active nanoparticles, variations in physicochemical properties and the surface properties of CNPs obtained from different synthesis methods can significantly affect their biological activity (inactive, antioxidant, or pro-oxidant). Moreover, these properties can influence the biological identity, cellular interactions, cellular uptake, biodistribution, and therapeutic efficiency. This review aims to highlight the critical role of various physicochemical and the surface properties of CNPs controlling their biological activity based on 165 cited references.

**ARTICLE HISTORY**
Received 13 November 2016
Revised 15 September 2017
Accepted 18 December 2017

**KEYWORDS**
Cerium oxide nanoparticles; physicochemical properties; surface properties; cellular uptake; sub-cellular localization; cytotoxicity

## Introduction

Cerium, a rare earth metal belonging to lanthanide series of the periodic table, has attracted considerable attention in the field of physics, chemistry, biology, and materials science due to its unique $[Xe]4f^15d^16s^2$ electronic configuration. Traditionally, soluble forms of cerium such as chloride, nitrate, and acetate salts have been used for biomedical applications such as immunomodulating, antitumor, bacteriostatic, bacteriocidal, and antiemetic agents [1,2]. In combination with oxygen, cerium adopts a crystalline fluorite lattice structure and its nanoscale counterpart (cerium oxide nanoparticles – CNPs) retains their fluorite structure with an oxygen vacancy being created upon the loss of lattice oxygen atoms due to a reduction in $Ce^{3+}$ ions [3–5]. Due to an increase in the surface-to-volume ratio, the CNPs possess relatively higher $Ce^{3+}$ contents than their micro-sized counterparts and eventually the atomic oxygen can move freely to fill the oxygen vacancies thereby providing oxygen mobility in the lattice for rapid generation of surface vacancy sites [6,7]. This fascinating property of CNPs provides facile switching between $Ce^{3+}$ ($Ce_2O_3$) and $Ce^{4+}$ ($CeO_2$) oxidation states with the CNPs surface being enriched with numerous active spots for redox reactions to occur [8,9]. Moreover, due to its oxygen buffering capacity, CNPs can self-regenerate to the initial $Ce^{3+}$ state without entering into any deleterious side reactions during regeneration [10,11]. Thus, CNPs finds wide industrial application as catalysts [12], UV screens [13], solar cells [14], fuel cells [15,16], gas sensors [17], etc. In biological applications, the CNPs are used primarily for scavenging surplus reactive oxygen species (ROS) and reactive nitrogen species (RNS) generated in human cells by mimicking natural antioxidant enzymes such as superoxide dismutase (SOD) and catalase (CAT) [18,19], as well as scavenging hydroxyl and nitric oxide radicals [20,21], thereby providing protection against trauma and aging [22,23],

CONTACT Bing-Huei Chen 002622@mail.fju.edu.tw Department of Food Science, Fu Jen Catholic University, New Taipei City 242, Taiwan
Supplemental data for this article can be accessed here.

Alzheimer's disease [24], ischemic stroke [25], cardiovascular disease [26], sepsis [27], diabetes [28], retinal damage [29,30], chronic inflammation [31], and cancer [32,33].

Generally, nanoparticles (NPs) are engineered to carry active compounds to the target-site overcoming biological barriers. However, the CNPs form a class of NPs in which the cerium oxide core by itself can act as a therapeutic material with reversible redox capability [7,34]. The antioxidant effect of CNPs is of utmost importance as the incidence of many chronic diseases can be closely associated with oxidative stress. The therapeutic use of CNPs provides multiple benefits over many antioxidant approaches including: antioxidants/enzymes-loaded NPs such as trolox- or glutathione-conjugated gold NPs, quercetin-encapsulated polylactide or poly(vinyl alcohol) polymeric NPs, chitosan-ascorbic acid NPs and SOD-loaded poly(lactic-co-glycolic acid) NPs [35]. Antioxidant-loaded NPs fail to scavenge more than one type of ROS and only a limited amount of antioxidant compounds can be loaded on such NP systems [36]. On the contrary, the CNPs possess the capability to scavenge multiple ROS such as superoxide anion radical, hydrogen peroxide, hydroxyl radical, nitric oxide radical and peroxynitrite anion [37,38]. For instance, the CNPs were shown to possess both SOD and CAT mimetic activity with their activity exceeding even endogenous enzymes [18,19]. Also, the CNPs at a concentration of 5.8 μM were able to provide a SOD equivalent to 527 U [39]. However, the choice of an appropriate dosage remains a big challenge in antioxidant therapy as basal ROS are required for proper cell and tissue functions [7,36]. While several studies have demonstrated the potential of CNPs to scavenge intracellular ROS and protect cell from damage [29,31,33,40,41], the pro-oxidant effects due to severe oxidative stress were also observed in some cell studies under physiologically relevant conditions [42–48]. Several other studies have shown CNPs to be catalytically inactive toward cells [49–51]. In addition, the selective inhibition of tumor cells without affecting normal cells was reported by several authors [52,53]. Although the CNPs have been reported to exhibit antioxidant activity at physiological pH [54] and pro-oxidant activity at acidic pH, the observed disparity in the biological effects of CNPs in several studies may be largely attributed to differences in physicochemical and surface properties of CNPs synthesized by various methods. This in turn can influence the biological identity (interaction of CNPs with various proteins in biological environment forming "protein corona"), leading to varying interactions with cellular constituents, biodistribution, and biological effects on cell organisms [55,56]. This review article has attempted to highlight various physicochemical and surface properties controlling the biological applications of CNPs.

## Electronic configuration and chemical composition

The chemistry of rare earth elements differs from other elements in the periodic table owing to shielding of 4*f* orbitals from the atom's environment by 4*d* and 5*p* electrons [57]. These orbitals provide rare earth elements with unique catalytic, magnetic, and electronic properties. Cerium is the first element in the lanthanide group with 4*f* electrons and its oxide in bulk form exists either as $CeO_2$ ($Ce^{4+}$) or $Ce_2O_3$ ($Ce^{3+}$) due to two partially-filled 4*f* and 5*d* orbitals (Figure 1(A)) [6]. However, at the nanoscale, both $Ce^{3+}$ and $Ce^{4+}$ coexist on the surface of CNPs attaining cubic fluorite structure with electronic configuration [Xe]$4f^1$ for the $Ce^{3+}$ form and [Xe] for the $Ce^{4+}$ form (Figure 1(B)). Structurally, the cerium atom in $CeO_2$ ($Ce^{4+}$) is surrounded by eight oxygen anions with each oxygen atom occupying a tetrahedral position, while the coexistence of $Ce^{3+}$ ions in nanoscale cerium oxide generates intrinsic oxygen defects due to compensation for a charge deficiency [58]. Consequently, CNPs can easily form non-stoichiometric composition ($CeO_{2-x}$) through conversion of a large number of $Ce^{4+}$ into $Ce^{3+}$ ions. Such oxygen defects increase following a decrease in particle size (Figure 1(C,D)) [6,59] or incorporation of trivalent dopant ions, which can act as "active centers" of various catalytic activities exhibited by CNPs (Figure 1(E)) [60]. Several techniques used for measuring the $Ce^{3+}/Ce^{4+}$ ratio on the CNP surface includes: X-ray photoelectron spectroscopy (XPS) [59], UV–visible absorption spectroscopy [61], X-ray absorption near-edge spectroscopy [6], and electron magnetic resonance spectroscopy [62].

## Redox capability and autoregenerative mechanism

Depending on the reaction conditions, CNPs exhibit a remarkable dual role as oxidation and reduction catalysts switching between $CeO_2$ and $CeO_{2-x}$ [62]. This redox cycle is formed mainly because of the low reduction potential (~1.52 V) of the $Ce^{3+}/Ce^{4+}$ couple [63]. The inherent oxygen defects in CNPs, caused by oxygen vacancies, are resistant to radical damage allowing a continuous autoregeneration to occur without any deleterious side reactions during regeneration [19,62,64,21]. In addition, the increased surface-to-volume ratio in

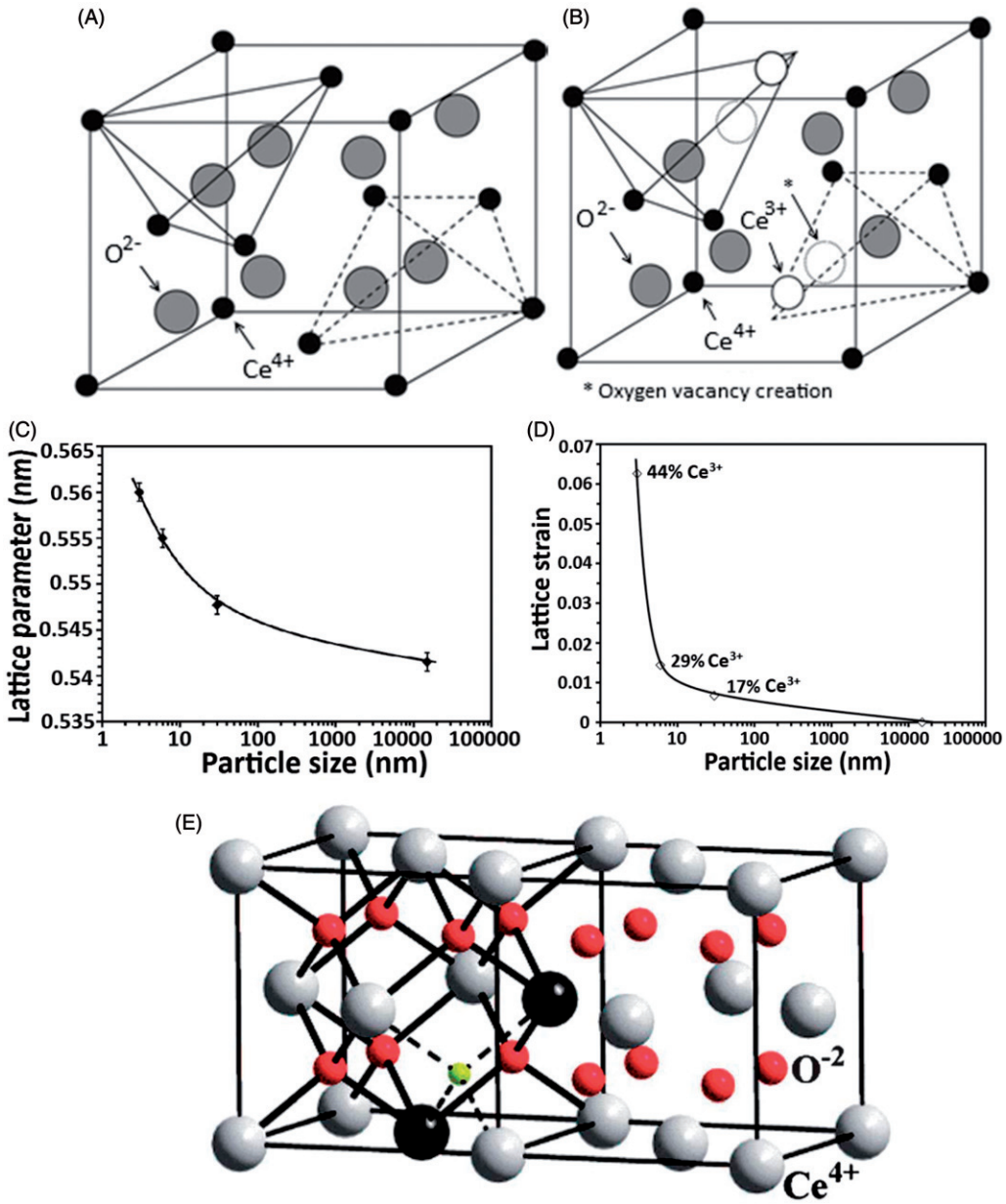


**Figure 1.** Schematic pictures showing bulk cerium oxide with intact fluorite structure (A) and CNPs with distorted crystal structure (B) due to creation of oxygen vacancy by replacement of some $Ce^{4+}$ ions with $Ce^{3+}$ ions. The panels (C) and (D) illustrates semi-log plot of a change in lattice parameter and lattice strain as a function of particle size with the latter (D) also indicating increasing $Ce^{3+}$ ions with decreasing size. The panel (E) depicts a schematic diagram illustrating oxygen vacancy creation (small spheres) after doping of trivalent ions from lanthanide series (dark spheres) on the left-side of cube, while the portion on right-side of cube shows undoped CNPs. (With permission from Deshpande et al. [6]; Sun et al. [89]).

CNPs and undisturbed fluorite structure during oxidation or reduction favors autoregeneration to its initial valence state [18,65]. Several studies have shown strong experimental evidence for the charge shift between $Ce^{4+}$ and $Ce^{3+}$ [66,67]. Moreover, microscopic techniques, including non-contact atomic force microscopy (NC-AFM) and high-resolution scanning tunneling microscopy (HR-STM), have also been employed for observing the dynamic behavior of surface oxygen atoms in CNPs. In two different studies, Fukui et al. [8] and Namai et al. [9] visualized the formation of hexagonally-arranged oxygen atoms with oxygen-terminated surface, oxygen point vacancies and multiple oxygen vacancies (triangular and line defects) by NC-AFM, providing an insight into the special oxygen storage capacity with facile oxidation–reduction cycles in CNPs. For stoichiometric $CeO_2$ {111} surface, the hexagonally arranged oxygen spots with enhanced brightness was observed, with the surface oxygen defects being visualized as isolated dark depressions. Application of HR-

STM revealed localization of electrons caused by oxygen release on cerium ions and oxygen vacancy cluster formation [3].

## Synthesis of cerium oxide nanoparticles

Over the past two decades, numerous synthesis methods have been explored for CNPs preparation, which includes hydrolysis [32,53], combustion/flame [68,69], precipitation [24,70–73], wet-chemical [31,34,74,75], sol–gel [76,77], hydrothermal/solvothermal [20,47,50,78,79] and microemulsion [25,37,80,81]. Some other methods such as thermal deposition [82], gas condensation [83], sonochemical [84], and electrochemical [85] were also used for synthesis of CNPs. Basically, the synthesis of solid NPs involves both nucleation and growth steps during their crystallization and nanocrystals of different shapes can be obtained by carefully adjusting several functional factors such as nucleating seeds, kinetic control and temperature [86,87]. Incorporation of capping materials can also significantly control the nanocrystal growth by altering activation energy on the surface. Both synthesis methods and conditions are critical, as the change in physical parameters such as particle size, shape, dispersion level, surface charge, surface coating, and residual surfactant contamination can influence the interactions at CNPs-biological interface. Most importantly, the manipulation of their surface $Ce^{3+}/Ce^{4+}$ ratio and oxygen vacancies significantly alters biological interactions [88]. While several comprehensive reviews on various synthesis methods and fundamental properties have been published elsewhere [89,90], the following section of this review unveils how CNPs can be tailored to possess various physicochemical characteristics for specific biological applications through appropriate selection of synthesis methods and conditions.

## Synthesis of CNPs with tailored physicochemical characteristics

CNPs with desired physicochemical parameters can be obtained by appropriate selection of synthesis methods. For example, wet-chemical and microemulsion methods provide good control over NPs size with the former yielding CNPs of small particle sizes without surface contamination [81,91]. The CNPs with surfaces free of contamination can also be obtained by employing spray pyrolysis and high temperature sintering methods. However, the latter method may produce crystalline, dense and agglomerated CNPs with large particle size (>25 nm) and fewer vacancies/defects [44,47]. Also, high-temperature synthesis methods involving sintering, calcinations, high-temperature/flame pyrolysis, and thermal decomposition generate CNPs with octahedron/truncated octahedron morphology with sharp facets or edges. Solvent-media based synthesis methods such as hydrothermal, solvothermal, and high-temperature hydrolysis yields smaller and uniform-sized CNPs which are often less agglomerated possessing spherical morphology [50]. However, a possible thin-layer deposition of a surfactant or solvent requiring additional surface characterization cannot be ignored for solvent-media synthesis methods. Room temperature synthesis methods including acid/base hydrolysis and microemulsion can produce CNPs with uniform size distribution, roughly spherical morphology and high $Ce^{3+}/Ce^{4+}$ ratio [92]. Nevertheless, they are less stable because particle size, surface charge, self-assembly, and oxidation state can be affected with changes in time, temperature, and environment. For other methods, an effective control in particle size can be attained by varying the reaction time in precipitation methods [93] and chain length of the coated polymer (polyvinylpyrrolidone) in hydrothermal methods [94], with the particle size showing an increased trend following a rise in the chain length for the latter method. Spherically shaped CNPs can be successfully synthesized by various methods including: wet chemical, microemulsion, reverse micelle, precipitation, acid/base hydrolysis, and hydrothermal/solvothermal methods [37,95]. Recent developments in synthesizing nanomaterials have enabled preparation of CNPs with different morphologies including: spheres, rods, cubes, wires, octahedrons, and polygonal [11,96–102].

The type of cerium salt and synthesis conditions can also play a key role in determining the size and morphology of CNPs, thereby affecting cytotoxicity. Several cerium salts used for synthesis such as cerium(III) sulfate, cerium(IV) sulfate, cerium(III) nitrate, and cerium(III) chloride were shown to significantly impact size and morphology, with pure nanorods being obtained only by using cerium(III) chloride [100]. As an additional oxidation step is usually required for $Ce^{3+}$ salt, the nucleation and crystal growth varies, which in turn alters the size and morphology making NPs much different from those obtained by using $Ce^{4+}$ salt [103,104]. More specifically, by adopting hydrothermal synthesis methods, the cerium(III) salt [$Ce(NO_3)_3{\cdot}4H_2O$] as a precursor was shown to yield coarse particles (160 Å), while cerium(IV) salts [$Ce(SO_4)_2{\cdot}4H_2O$ and $Ce(NH_4)_4(SO_4)_2{\cdot}2H_2O$] produced a fine powder (30 Å) (Figure 2(A–C)) [103]. The counter anions in cerium salts can also play a vital role in controlling both size and morphology. For example, the synthesis method employing cerium salts with counter anions $SO_4^{2-}$, $Cl^-$, $Br^-$, and $I^-$ promoted

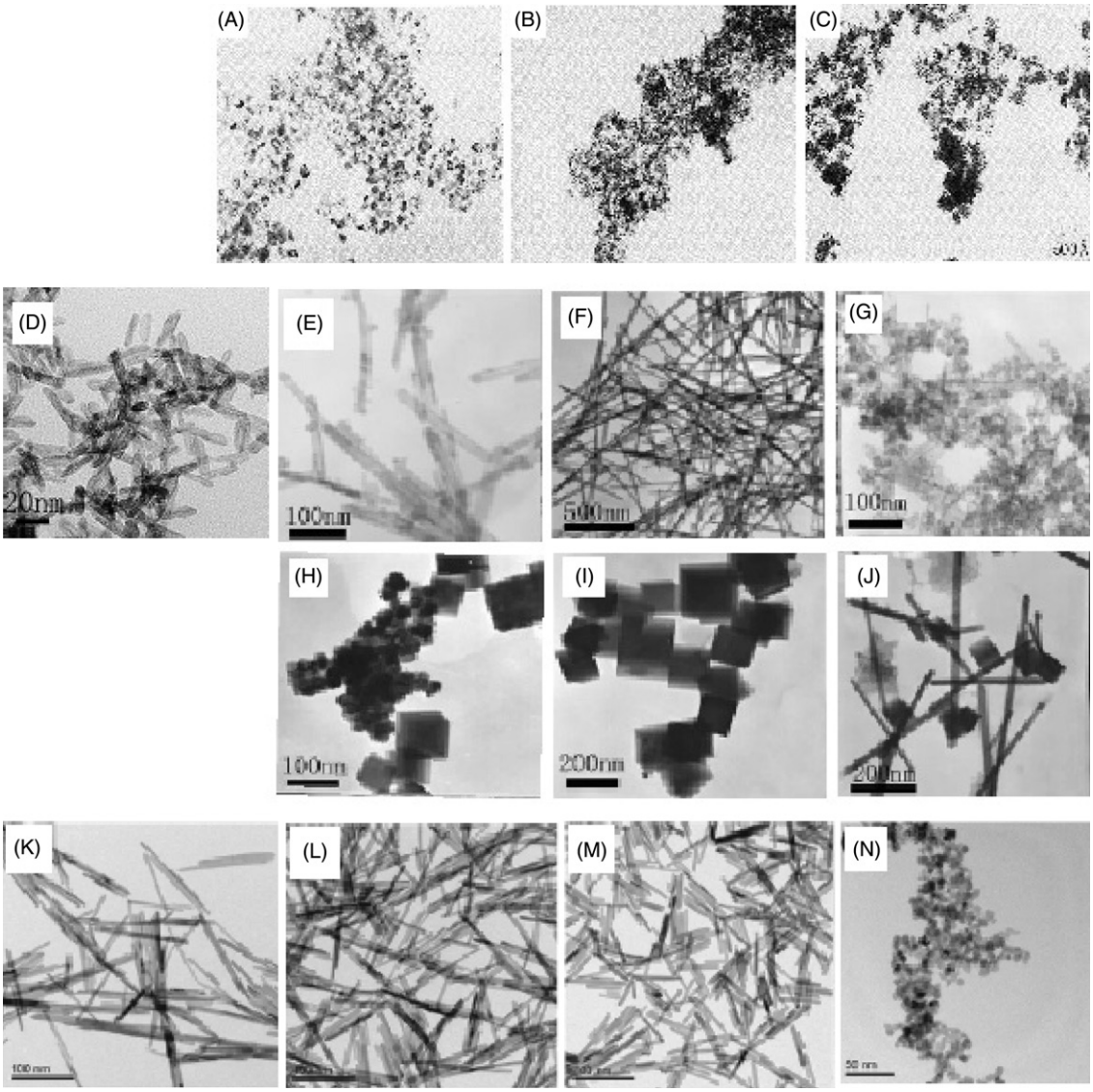


**Figure 2.** TEM images of CNPs obtained as coarse particles from Ce(III) salt [$Ce(NO_3)_3{\cdot}4H_2O$] as precursor (A) and fine powders from Ce(IV) salts [$Ce(SO_4)_2{\cdot}4H_2O$ and $Ce(NH_4)_4(SO_4)_2{\cdot}2H_2O$] (B,C) under hydrothermal conditions at 180 °C for 5 h. The panels D–J show the TEM images of cerium oxide nanorods obtained by hydrothermal method at 20 °C (24 h) (D) and their conversion to nanotubes at 100 °C (72 h) (E), nanowires at 110 °C (24 h) (F), nanospheres at 120 °C (24 h) (G), nanospheres and nanocubes at 140 °C (24 h) (H), and nanocubes at both 160 °C and 180 °C (24 h) (I,J). The panels K, L, and M depict TEM images of cerium oxide nanorods obtained by hydrothermal method at 220 °C using $CeCl_3$ as precursor at pH 1.8, 2.5, and 4.0, respectively, while the panel N shows formation of nanocubes at pH 11.8. (With permission from Hirano and Kato [103]; Pan et al. [104]; Ji et al. [100]).

formation of nanorods, while that with $NO_3^-$ anion favored nanocube formation [105]. In addition, $Cl^-$ anions in cerium salts can be adsorbed onto the surface of $Ce(OH)_3$ nanorod nuclei stabilizing the nanorod/nanowire structure, with the length of nanorods becoming shorter upon increasing the $CeCl_3$ concentration. Incorporation of phosphate ions also plays a key role in promoting the formation of nanorods under acidic condition [100]. The effect of reaction temperature on different CNPs morphology is quite complicated and inconsistent as CNPs with different morphologies can be obtained at the same temperature depending on reaction time and composition of synthesis mixtures. Pan et al. [104] synthesized nanorods at room temperature (20 °C) by a hydrothermal method and demonstrated their conversion to nanotubes at 100 °C (72 h), nanowires at 110 °C (24 h), nanospheres at 120 °C (24 h), nanospheres and nanocubes at 140 °C (24 h), and nanocubes at both 160 and 180 °C (24 h) (Figure 2(D–J)). However, Ji et al. [100] pointed out that the nanorods synthesized by the hydrothermal method were stable at all synthesis temperatures (140–240 °C) even after a

72 h reaction time, with the nanorods becoming shorter due to faster nucleation at elevated temperatures. Upon using seed crystals from primary synthesis for secondary hydrothermal treatment yielded nanowires or nanorods at 220 °C. Moreover, the nanorods were formed only under acidic conditions (pH 1.8, 2.5, and 4.0), with their length becoming longer at a lower pH while, at pH >10 (11.8), only nanocubes were formed (Figure 2(K–N)). Thus, the use of different types of cerium salts and synthesis conditions can yield NPs of varying size and morphology, and eventually exert different cytotoxic effects.

The level of dispersion is another important factor to be considered during CNPs synthesis as it determines the extent of agglomeration in water and biological media. Most importantly, a rise in dispersion levels of NPs not only increase stability, but also reduce non-specific interactions with cells and proteins. Also, it prolongs blood circulation time, mitigates NPs toxicity, and lowers effective dose to minimize side-effects. It has been well documented that the degree of dispersion can be largely improved by coating CNPs with biocompatible polymers, surfactants, composite materials, stabilizers, or biomacromolecules during or after synthesis. Several CNPs were synthesized by coating with a biocompatible polymer such as dextran [106,107], poly(acrylic acid) [71], polyethylene glycol [108], and polyethyleneimine [109] or other surfactants/stabilizers such as citric acid [79], oleic acid [109], hexamethylenetetramine [11], 2-ethylhexanoic acid [110], and sodium bis(2-ethylhexyl)sulphosuccinate [81]. As a result of coating, the surface charge of CNPs can be greatly increased, which is an important aspect to be considered for biological applications, as the stability, uptake mechanism, and intracellular localization of CNPs in different cell compartments and eventual cytotoxicity depends on CNPs' surface charge [70,71,111]. The high degree of CNPs dispersion can also affect protein absorption in cell culture media and in *in vivo* environment leading to formation of protein corona, which in turn dictates the cellular uptake and clearance from body (please refer to "biological identity" in Supplementary Information) [112].

The surface oxidation state ($Ce^{3+}/Ce^{4+}$ ratio) is very important for the redox catalytic activity and biomedical application. For instance, CNPs with a higher $Ce^{3+}/Ce^{4+}$ ratio or oxygen vacancy are shown to be protective against diseases associated with oxidative stress or inflammation because of their superior SOD mimetic activity. On the contrary, CNPs with lower $Ce^{3+}/Ce^{4+}$ ratio exhibit anticancer and antibacterial activities due to their higher CAT-mimetic activity [88]. The ratio of $Ce^{3+}/Ce^{4+}$ on CNPs surface can vary depending upon the synthesis conditions which are discussed in the following sections.

## Tuning of surface oxidation state

The synthesis of CNPs with a tunable $Ce^{3+}/Ce^{4+}$ ratio is pivotal for specific biological application. A correlation between particle size and lattice parameter was established by Deshpande et al. [6], who reported an increase in $Ce^{3+}$ ion concentration due to lattice strain caused by oxygen vacancies on CNP surface, accompanied by reduction in particle size from 30 nm to 3 nm and elevation of $Ce^{3+}$ level from 17% to 44%. In other words, the smaller the CNPs particle size, the higher the surface $Ce^{3+}/Ce^{4+}$ ratio. The surface oxidation state can also vary depending on synthesis methods and conditions. Accordingly, the synthesis methods carried out at high temperatures yield CNPs with lower $Ce^{3+}/Ce^{4+}$ ratio and larger particle size. For example, the $Ce^{3+}/Ce^{4+}$ ratio for europium-doped CNPs synthesized by a co-precipitation method was reported to decrease from 23.5% to 14.0% after high-temperature annealing treatment [113]. However, the CNPs with higher $Ce^{3+}/Ce^{4+}$ ratio can be prepared by using the synthesis methods carried out at room temperature [108,114] or by irradiation [115]. Different chemicals such as hexamethylenetetramine, sodium hydroxide, or ammonium hydroxide used during synthesis were shown to produce CNPs with lower $Ce^{3+}/Ce^{4+}$ ratio (21–30%) [11], while CNPs with higher $Ce^{3+}/Ce^{4+}$ ratio (55–65%) could be obtained by using hydrogen peroxide [91]. Also, through treatment of CNPs with ascorbic acid, a high surface $Ce^{3+}/Ce^{4+}$ ratio could be attained [75].

Additionally, the reaction of CNPs with elements such as zirconium (Zr) and platinum (Pt) could lead to an increase in surface $Ce^{3+}/Ce^{4+}$ ratio. Zhang et al. [59] observed an increased $Ce^{3+}$ level in zirconia-doped ceria prepared under an oxidizing environment, with an increase in zirconia level from 60% to 94% rising the proportion of $Ce^{3+}$ ions by 83%. The underlying mechanism involves conversion of $Ce^{4+}$ to $Ce^{3+}$ compensating for the local strain caused by smaller $Zr^{4+}$ ions in the cubic phase of nanoparticles. In a later study, the incorporation of platinum nanoparticles onto a ceria film was shown to increase the $Ce^{3+}$ level through two coexisting interaction mechanisms, i.e. electron transfer from Pt to ceria and activated oxygen transport from ceria to Pt, with the latter alone contributing to a 40% increase in $Ce^{3+}$ level [116].

During biologically relevant conditions *in vitro*, Singh et al. [117] determined the shift in redox state of CNPs and their eventual effects on catalytic properties as affected by different pH conditions, biological media,

buffers, and ions. The CNPs remained unchanged in both the redox state and catalytic activity when exposed to different pH conditions (pH 3–9), DMEM medium, and other ions (sulfates and carbonates). However, the treatment of CNPs with 100 μM phosphate buffer (pH 7.4) reversed the redox state by decreasing the $Ce^{3+}$ leading to a complete loss of SOD mimetic activity, accompanied by a rise in CAT mimetic activity. Thus, an appropriate tuning of the surface oxidation state of CNPs is critical as pointed out by Pulido-Reyes et al. [118] that a shift from superoxide dismutase activity to catalase mimetic activity can occur in a narrow range of the surface $Ce^{3+}$ level between 40% and 30%.

## Trivalent metal dopants for tuning $Ce^{3+}/Ce^{4+}$ ratio

Several trivalent metal ions such as europium (Eu), neodymium (Nd), samarium (Sm), gadolinium (Gd), erbium (Er), ytterbium (Yb), lanthanum (La), holomium (Ho) thulium (Tm), terbium (Tb), and yttrium (Y) have also been used as dopants for tuning oxygen vacancy concentrations and $Ce^{3+}/Ce^{4+}$ ratio on CNPs surface for application in a broad range of fields including catalysis, biomedicine, electronics, and environmental sensing. Patil et al. [119] synthesized La- and Nd-doped CNPs in the particle size range of 3–5 nm by a microemulsion technique and found that their oxygen defect levels followed an increased trend compared to non-doped CNPs, implying a higher $Ce^{3+}/Ce^{4+}$ ratio on CNPs surface could occur when doped with La or Nd. Moreover, due to a larger ionic radius, doping with La was shown to produce a higher $Ce^{3+}/Ce^{4+}$ ratio on CNPs surface than doping with Nd. By employing the same method, Babu et al. [120] prepared Sm, Gd, Yb, and Y-doped CNPs (3–5 nm) and demonstrated an increase in oxygen defect and $Ce^{3+}/Ce^{4+}$ ratio for these CNPs. But for Yb-doped CNPs, a suppression in the formation of oxygen vacancy was observed due to a smaller ionic radii of $Yb^{3+}$ ion (0.0985 Å) compared to that of Sm (0.1079 Å), Gd (0.1053 Å), and Y (0.1019 Å), suggesting that by doping with suitable trivalent ions differing in ionic radii, the oxygen vacancy and $Ce^{3+}/Ce^{4+}$ ratio can be tuned for specific catalytic and biological application. In another study, the multicolored redox active CNPs obtained by multi-metal doping of CNPs with 20% Yb +2% Er, 20% Yb +2% Ho, and 20% Yb +0.5% Tm were shown to selectively inhibit lung cancer cells CRL-5803 without affecting normal cells (HUVEC and WI-38) [52]. More recently, Wang et al. [75] illustrated that the high ROS scavenging ability was due to high $Ce^{3+}/Ce^{4+}$ ratio obtained by doping CNPs with Tb. A similar rise in $Ce^{3+}/Ce^{4+}$ ratio was also reported by Shehata et al. [121], synthesizing CNPs doped with both Sm and Nd. However, an opposite trend was shown when doped with Ho and Er. Figure 3 shows XPS spectrum showing representative deconvoluted peak-fits of Ce(3d) for pure dextran-CNPs, 15 mol% europium-doped CNPs, 20 mol% erbium-doped CNPs, 20 mol% lanthanum-doped CNPs and 20 mol% samarium-doped CNPs, all of which indicated an increase in $Ce^{3+}$ ions upon doping with trivalent ions from the lanthanide series.

Interestingly, a contradictory result was reported by Dunnick et al. [122], who observed a decrease in antioxidant potential upon doping of CNPs with Gd. More elaborately, 10% Gd- and 20% Gd-doped CNPs with a comparable $Ce^{3+}$ level of 42% and 44%, respectively, were shown to exhibit different scavenging abilities towards hydroxyl radicals, which can be due to the stability of Gd in the lattice structure, thereby preventing the transition between two oxidation states ($Ce^{3+}$ and $Ce^{4+}$). This phenomenon revealed that the transition ability between $Ce^{3+}$ and $Ce^{4+}$ is even more important than the $Ce^{3+}/Ce^{4+}$ ratio. Also, while both 10% Gd- and 20% Gd-doped CNPs significantly reduced the hydroxyl radicals in rat alveolar epithelial cell RLE-6TN, only the former could scavenge free radicals generated in rat alveolar macrophage cell NR8383, which should be due to differences in cellular physiology and function.

Europium (Eu), a rare earth metal capable of emitting strong red light upon doping in different matrices, is also considered a suitable dopant for three main reasons: (1) it can be excited from ultraviolet light to visible light, (2) the ionic radius of $Eu^{3+}$ (0.1066 Å) is close to cerium (0.1143 Å for $Ce^{3+}$ and 0.097 Å for $Ce^{4+}$), and (3) it increases the trivalent state on the CNPs surface [113]. Several studies have shown pronounced emission after doping CNPs with Eu exhibiting a photoluminescence property. For instance, Li et al. [123] synthesized 0.1–10% Eu-doped CNPs by sol–gel methods and attributed the presence of broad band in the excitation spectrum to a charge transfer transition from $O^{2-}$ to $Ce^{4+}$ and not from $O^{2-}$ to $Eu^{3+}$. Likewise, an increase in both oxygen vacancy concentration ($1.61 \times 10^{20}$ to $4.03 \times 10^{20}$ $cm^{-3}$) and $Ce^{3+}/Ce^{4+}$ ratio (18.3–23.5%) was shown following a rise in Eu doping from 1 to 30 mol% in CNPs [113]. More recently, Vinothkumar et al. [124] demonstrated continuous protection of methyl violet through scavenging of hydroxyl radicals by Eu-doped CNPs synthesized at 1:1 ratio of fuel (cerium nitrate and europium nitrate) to oxidizer (glycine). It was shown that the doping of Eu could promote extrinsic oxygen vacancies and defect concentration, thereby increasing the concentration of highly reactive $Ce^{3+}$ for enhanced antioxidant potential.

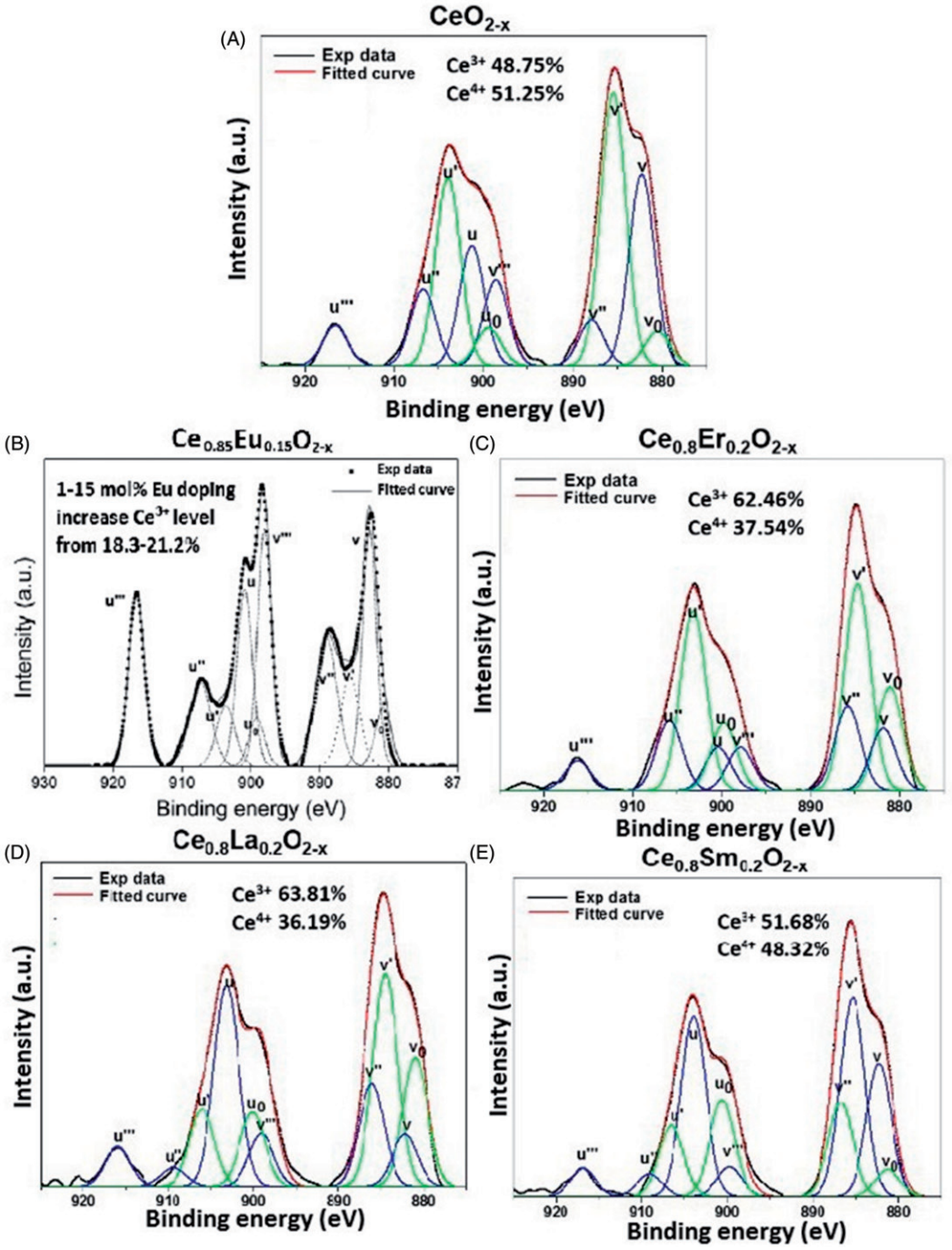


**Figure 3.** XPS spectrum showing representative deconvoluted peak-fits of Ce(3*d*) for pure dextran-CNPs (A), 15 mol% europium-doped CNPs (B), 20 mol% erbium-doped CNPs (C), 20 mol% lanthanum-doped CNPs (D) and 20 mol% samarium-doped CNPs (E), all of which indicating increase in $Ce^{3+}$ ions upon doping with trivalent ions from lanthanide series. $v_o$, v′, $u_o$, and u′, peaks corresponding to $Ce^{3+}$ ions. v, v″, v‴, u, u″, and u‴, peaks corresponding to $Ce^{4+}$ ions. (With permission from Gupta et al. [88]; Kumar et al. [113]).

Erbium (Er) is another rare earth metal which can act as an efficient up-conversion optical center. The electron transition between $Er^{3+}$ and CNPs occurs through two main mechanisms, the first involving both ground-state and excited-state absorption processes and the second involving energy transfer up-conversion process [125]. By adopting a reverse micelle synthesis technique, Woan et al. [126] prepared 1–10 mol% Er-doped CNPs and demonstrated a 1.45-fold higher $H_2O_2$ catalytic activity for 10 mol% Er-CNPs compared to pure CNPs, which can be attributed to increased oxygen vacancy caused by substitution of two erbium atoms on

each cerium site. Such vacancy provides active sites for oxidative species to undergo catalytic reaction for execution of antioxidant activity. On the contrary, doping of CNPs with Sm, a metal similar to Er in valence and redox state, was reported to impair both antioxidant and anti-apoptotic ability towards human macrophage U937 cells, implying that doping with Sm can tailor the CNPs surface with a reduction in $Ce^{3+}$ ions without affecting the oxygen vacancy [34]. The outcomes of this study is critical as numerous studies have suggested a correlation between oxygen vacancy and increased $Ce^{3+}$ ion concentrations. More recently, Gupta et al. [88] prepared Er-, Sm-, or La-doped CNPs and CNPs capped with dextran by precipitation method for tuning the $Ce^{3+}/Ce^{4+}$ ratio. Based on XPS analysis, a rise in $Ce^{3+}$ level up to 40% was observed in doped CNPs as compared to the control (dextran-capped CNPs), with each $Ce^{3+}$ oxidation state generating two oxygen vacancies. The CNPs doped with Sm was shown to possess the highest SOD-mimetic activity, followed by La and Er, while an opposite order was found for the CAT-mimetic activity. The findings shown above should be closely associated with the dopant's association energy of oxygen vacancies and their ability to raise $Ce^{3+}$ level on CNPs surface by following the order: Sm > La > Er.

Collectively, the incorporation of rare earth metals into CNPs structure favors an increase in oxygen vacancy levels through creation of a non-stoichiometric condition by reduction of $Ce^{4+}$ to $Ce^{3+}$, thereby facilitating the tuning of CNPs' ionization state and its oxygen vacancy for a wide range of applications.

## The size and shape of CNPs on cytotoxicity

Both size and shape of nanoparticles are critical factors in determining the toxicity of any nanomaterial as their variation can cause different degrees of cellular uptake and toxicity. The smaller CNPs have the potential to exhibit higher toxicity because of their larger surface-to-volume ratio, higher $Ce^{3+}$ level and faster kinetics to attain higher cellular uptake. For example, 3.8 nm oleic acid-coated CNPs with higher $Ce^{3+}$ content (44%) was shown to quench more $H_2O_2$ than 8.2 nm CNPs with 30% $Ce^{3+}$, and the former could reduce $H_2O_2$-induced oxidative stress in human dermal fibroblast cell GM00498 to a larger extent (Supplementary Figure S1A) [109]. Kumari et al. [127] also compared the cytotoxicity of CNPs with different size towards neuroblastoma cells and found that the nano-sized $CeO_2$ particles (25 nm) exhibited higher toxicity than the micro-sized particles (3 μm). More recently, differential genomic effects exerted by two different commercial CNPs with particle size 8 nm (S) and 58 nm (L) were reported by Thai et al. [128], who demonstrated that the former exhibited stronger antioxidant activity than the latter, probably due to a higher $Ce^{3+}$ level and a large surface area per unit weight. Most importantly, the S-CNPs were shown to cause the Warburg effect towards human liver hepatocellular carcinoma HepG2, while the L-CNPs did not cause any effect. Moreover, the S-CNPs was more effective than L-CNPs in altering pathways of mitochondria dysfunction, apoptosis, epithelial adherens junction signaling, acute phase response, actin nucleation by ARP-WASP complex, and TCA cycle as well as elevating fatty acid levels by metabolomics. However, the L-CNPs were more effective than S-CNPs with respect to pathways of hepatic fibrosis/hepatic stellate cell activation and NRF2-mediated stress response. On the contrary, Peng et al. [129] found CNPs with 3–5 nm to exhibit similar cytotoxicity as 6.6 nm mainly due to agglomeration of the former.

The size-independent toxicity effects of CNPs were also reported by several authors. Schubert et al. [74] reported that all the three CNPs at 6 nm, 12 nm, and micron-size were neuroprotective without significant difference upon treatment with the HT22 hippocampal nerve cell line. In another study, four different CNPs (15, 25, 30, and 40 nm) synthesized by the supercritical method did not exhibit significant difference in toxicity towards human bronchus epithelial cells BEAS-2B even after 96 h of incubation [130]. Regardless of particle size, the three CNPs at 7, 14, and 94 nm were shown to be effective in reducing intracellular ROS in both U937 and activated U937 cells [131]. An insignificant difference in cytotoxicity may partly be attributed to aggregation of CNPs in cells, thereby reducing the differences in surface area between CNPs of different sizes. Based on the interaction with living matter, the NPs of size <100 nm in diameter can enter into cells. More specifically, the NPs <40 nm can enter into the nucleus, while those <35 nm in size can cross the blood-brain barrier [132]. However, this rule cannot be generalized for all NPs and cells, as the same type of NPs are likely to interact differently depending on cell types and internalization through different uptake mechanisms. Several other factors such as unique phenotypes, membrane fluidity, cell cycle, and target receptor may also affect the cells' interaction with NPs.

The CNPs of the same particle size, obtained by two different synthesis routes, can also exhibit varying toxicity depending on their agglomeration tendency. According to the classification of CNPs' tendency to form agglomerates based on their synthesis methods by Karakoti et al. [95], the CNPs obtained by high temperature synthesis methods (>300 °C) tend to form hard and large agglomerates. However, those obtained

by solvent-based low temperature heating (<100 °C) and room temperature methods are less prone to agglomeration. In addition, the biological activity of CNPs obtained by high-temperature methods shows predominantly pro-oxidative effects, while those by solvent-based low temperature methods provides little or an ambiguous response, and room temperature methods show mostly an anti-oxidative response. However, this trend is not universal for all the toxicity studies of CNPs. For instance, Renu et al. [53] have shown CNPs of similar size (100–115 nm) synthesized by two different synthetic routes (hydrothermal and precipitation) to possess different morphology (flaky and spherical) and stoichiometry ($CeO_2$ and $Ce_2O_3$) (Supplementary Figures S1B and S2C), with those obtained by the former method showing a more pronounced cellular uptake and cytotoxic effect towards PC-3 human prostate cancer cells (Supplementary Figure S1D). This outcome may be due to a relatively higher agglomeration of CNPs obtained by hydrothermal method than by precipitation method. Similarly, two different CNPs of the same size (3–5 nm), synthesized by precipitation and hydrothermal methods were reported to induce pulmonary toxicity through different mechanisms. More elaborately, CNPs synthesized by the precipitation method induced acute inflammation due to a larger number of small aggregates and high deposition rate in the lungs, and the high reactivity of CNPs by the hydrothermal method generated ROS causing inflammation and cytotoxicity in the early stage as well as lipid peroxidation and pro-inflammation in the latter stage [129]. In other words, the difference in toxicity mechanism can be caused by variations in the agglomeration nature as the CNPs obtained by the hydrothermal method can generated large agglomerates, while those by precipitation method can produce small aggregates.

To reduce CNPs agglomeration, the synthesis method through incorporation of coating materials such as polymer or surfactants has been shown to be promising. Lee et al. [109] demonstrated that the stability of poly(acrylic acid)- or oleic acid-coated CNPs could be enhanced as it can be repeatedly used for several months through preservation of antioxidant activity by sustaining redox-cycling process up to 20 cycles in the presence of high $H_2O_2$ concentration. In addition, the 3.8 nm CNPs with a thinner coating of poly(acrylic acid)/oleic acid was able to quench more $H_2O_2$ than 8.2 nm CNPs with a thicker coating of polyethylene imine or polymaleicanhydride-alt-1-octadecene, implying that the coating thickness can also play a significant role in dictating antioxidant activity. In another study, CNPs coated with a mixture of citrate and EDTA (2.9 nm) was reported to remain monodispersed in physiological solutions, resist agglomeration even after centrifugation, bind minimum protein and prolong plasma half-life 4 times compared to similar-sized CNPs coated with only citrate [133]. Nevertheless, the synthesis with or without coating material may not be the only determining factor, as difference *in vitro* and *in vivo* conditions such as biological buffer, pH, and ionic strength as well as the interaction mechanism between CNPs and protein or cell components can also influence the degree of agglomeration.

Apart from the particle size, shape can also be a determinant factor in affecting cytotoxicity. NPs with a wide variety of shapes such as spheres, pillars, helices, cubes, rods, wires, polygonal, octahedral, and some other irregular shapes have been reported [87,89,134]. Due to their elongated structure, these high aspect ratio NPs (HAR-NPs) exhibit different chemical, electrical, magnetic, and optical properties, thereby interacting with cells and biomolecules through different mechanisms [100]. Synthesis of one-dimensional $CeO_2$ nanostructures such as nanorods, nanowires, and nanotubes has attracted attention because of their high redox and catalytic activities. In a recent study, Wang et al. [135] compared the toxicities of nanocubes, nanooctahedra, and nanorods of CNPs towards HepG2 cells, the highest toxicity was reported for nanocubes, followed by nanooctahedra and nanorods, along with their specific surface area being 18.9, 29.9, and 83.2 $m^2/g$, respectively (Figure 4(A)). Furthermore, the CNPs possessing a smaller specific surface area was shown to induce more apoptosis, increase mitochondria membrane potential, ROS and glutathione, and lower the cells capability to scavenge hydroxyl free radicals. However, in a similar study, only three nanorods with a different surface area (37–151 $m^2/g$), but not nanooctahedra and nanocubes of comparable surface area (60 $m^2/g$), were shown to exhibit toxicity in terms of lactose dehydrogenase release and TNF-α production in a dose-dependent manner towards RAW264.7 cells (Figure 4(B)) [136]. In another study, CNPs of different shapes, nanospheres and nanorods were reported to scavenge more ROS than nanowires due to internalization of a higher amount of nanospheres and nanorods within 24 h (Figure 4(C)) [137]. However, the highly elongated nanowires initially scavenged ROS extracellularly and then followed an increased internalization after 48 h incubation (Figure 4(D)). A schematic diagram in Figure 4(E) depicts intracellular ROS scavenging by nanospheres and nanorods within 24 h, while more extracellular scavenging by nanowires. It may be postulated that the difference in toxicity trend shown above should be due to variation in some other physicochemical characteristics of CNPs and

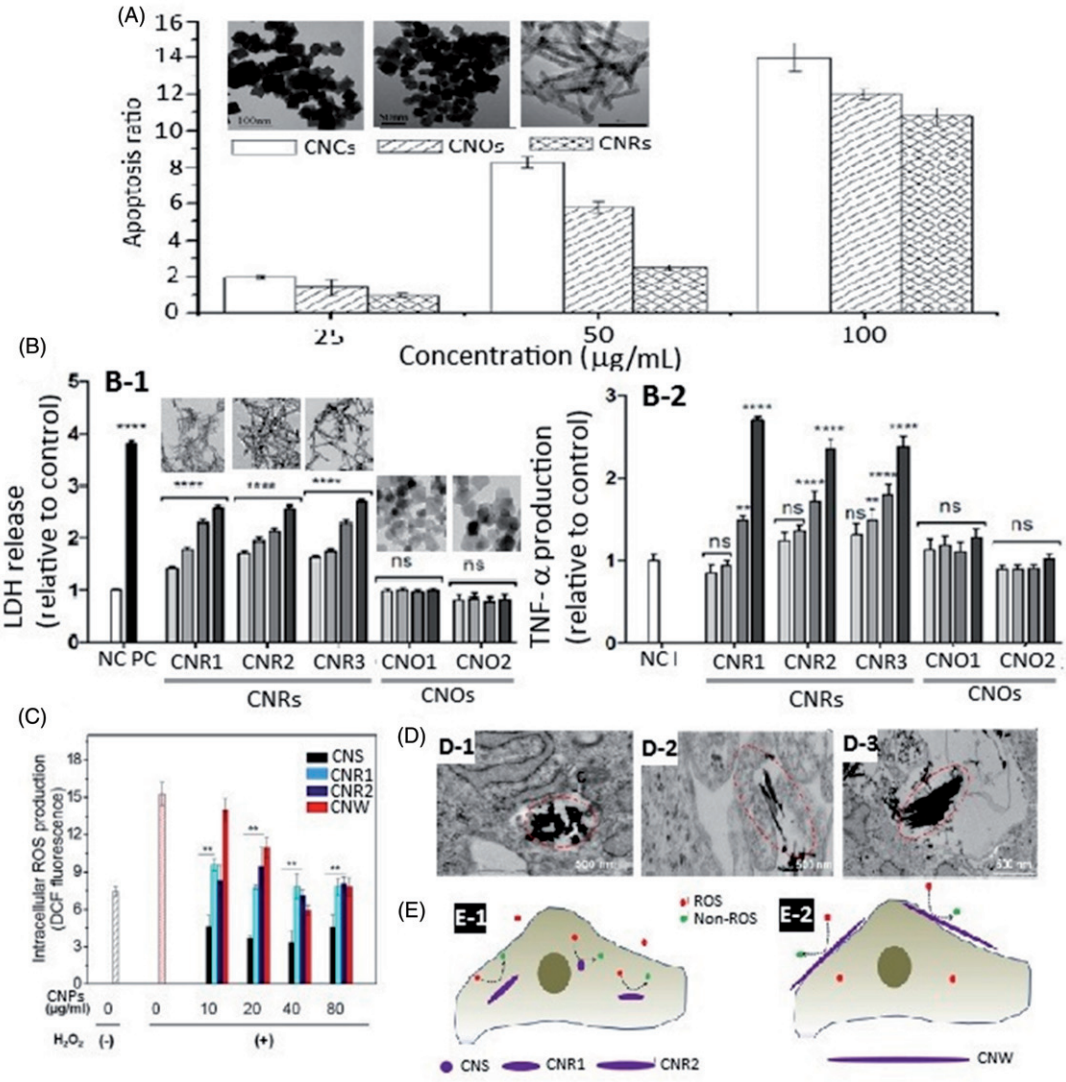


**Figure 4.** Effect of different shapes of CNPs on cytotoxicity and intracellular ROS scavenging. The panel (A) depicts percentage apoptosis of human hepatacellular carcinoma cell HepG2 after treatment with nanocube (20–50 nm), nanooctahedron (10–30 nm) and nanorod (8 × 100–400 nm)-shaped CNPs at different concentrations (25, 50, and 100 μg/mL synthesized by hydrothermal method along with their TEM images shown in the inset. The panel (B) shows release of lactose dehydrogenase (LDH) release (B-1) and tumor necrosis factor-alpha (TNF-α) production (B-2) upon incubating three differently-sized CNRs (CNR1: 44 × 5.5 nm, CNR2: 45 × 6.2 nm, CNR3: 70 × 8.1 nm) and CNOs (CNO1: 11.3 nm, CNO2: 16.2 nm) with mouse macrophage cell RAW 264.7 with inset showing their TEM images as well. PC: positive control of cells treated with Triton x100. NC: negative control with untreated cells. ns: not significant. The panel (C) reveals cellular ROS levels before and after treatment of human dental stem cells with $H_2O_2$, cerium oxide nanospheres (CNS: 20 × 19.3 nm), small-sized nanorods (CNR1, 107.8 × 12.4 nm), medium-sized nanorods (CNR2, 250 × 20.7 nm) and nanowires (CNW, 537.3 × 21.8 nm). The panel (D) shows internalization of nanospheres in human dental stem cells after 24 h treatment (D-1), less amount of CNWs after 24 h treatment (D-2), and more amounts of CNWs after 48 h treatment (D-3). The panel (E) is a schematic diagram illustrating possible shape-dependent mechanism of rapid intracellular ROS scavenging by CNS, CNR1 and CNR2 after 24 h treatment (E-1) as well as initial extracellular ROS scavenging by CNWs (E-2). (With permission from Wang et al. [135]; Forest et al. [136]; Mahapatra et al. [137]).

cell type, as the CNPs with different morphologies possessing varying crystal facets may also influence stability and reactivity. For example, Naganuma [102] synthesized nanopolyhedra, nanocube, and nanorod CNPs synthesized with particular crystal planes and a specific surface area, {111}/{100} and 82.4 $m^2$/g, {100} and 93.2 $m^2$/g, and {111}/{100} and 163.7 $m^2$/g, respectively, a low toxicity towards the human promyelocytic leukemia cells HL60, along with enhancement of catalase mimetic activity by nanopolyhedra containing a high level of $Ce^{4+}$ was observed, while both nanocubes and nanorods with a high level of $Ce^{3+}$ could promote SOD mimetic activity.

In an attempt to evaluate the optimal length (*L*) and aspect ratio (*R*) of HAR-NPs for causing cytotoxicity, Ji et al. [100] prepared cerium oxide nanorods and

nanowires by a hydrothermal method and reported that the short $CeO_2$ nanorods with lower aspect ratios ($L = 33.2–106.7$ nm, $R = 1–16$) remained non-toxic towards the human myeloid cell THP-1, while the long $CeO_2$ nanorods with intermediate aspect ratio ($L = 197.2$ and 310.4 nm, $R = 22$ and 31) induced IL-1β production without cell death. However, two longer nanowires with high aspect ratio ($L = 495.7$ and $>1000$ nm, $R = 52$ and $>100$) showed significantly higher cell death rate than shorter nanorods, with the critical length and aspect ratio leading to lysosomal damage were identified to be 200 nm and 22, respectively. This critical dimension responsible for toxicity was mainly due to the formation of stacking bundles for thin (6–10 nm) nanorods/nanowires through van der Waals force and dipole-dipole attractions between parallel-aligned nanorods/nanowires. In a later study, Lin et al. [101] demonstrated that the long HAR $CeO_2$ nanorods ($L \geq 1000$ nm, $R \geq 100$) could induce significant IL-1β and TGF-β1 production *in vivo* in the bronchoalveolar lavage fluid after 21 days and more collagen production after 44 days in mouse lung when compared to nanorods of shorter aspect ratio ($L = 50.8–495.7$ nm, $R = 8–52$) and nanospheres (7 nm). Furthermore, they were shown to cause serious injury in the epithelial lining of gastrointestinal tract of zebrafish larvae resulting in a significant growth inhibition, decrease in body weight, and delayed vertebral calcification. However, both nanospheres and shorter nanorods failed to show any significant effects [101]. Additionally, studies have also shown that with the exception of spheres, CNPs with specific morphology, can mechanically damage cells due to their sharp edges. For instance, the high-aspect ratio cerium oxide nanorods showed progressive pro-inflammatory effects and cytotoxicity towards human myeloid cell THP-1 through lysosomal damage and IL-1β production [100]. On the contrary, no significant difference in HUVEC cell viability was observed for hexamethylenetetramine (HMT)-coated CNPs with polygonal shape and sharp edges when compared to HMT-CNPs with round shapes [11].

Taken together, both size and shape of NPs are important parameters for an evaluation of cytotoxicity. As a general rule, the smaller the size of NPs, the larger the surface-to-volume ratio and the greater surface area for the cells to interact. Also, NPs with smaller size are enriched with $Ce^{3+}$ ions which are capable of scavenging both cellular and intracellular ROS [131]. Conversely, some studies have shown the capability of CNPs to induce toxicity in SMMC-7721 human hepatoma cells regardless of size and morphology [138,139]. Accordingly, the small-sized NPs possessing high surface area should be more toxic than the large-sized ones. However, the observed inconsistency may be due to aggregation of CNPs which reduces the toxicity difference among differently-sized CNPs. On the other hand, the HAR-CNPs possess a high oxygen storage capacity and superior reduction capability, with the longer ones eliciting greater cytotoxicity than their shorter counterparts. However, the nanowires, being highly elongated, may exhibit toxicity only at prolonged incubation times due to their slow entry into the cell as reported by Mahapatra et al. [137]. Thus, the effect of size and morphology of CNPs on cytotoxicity does not seem to provide uniform results, as the interaction mechanism not only depends on the properties of CNPs but also on the cell culture environment and cell type.

## Effect of CNPs' surface charge on cytotoxicity

Besides size and morphology, the surface charge of CNPs plays a pivotal role in cell targeting, cell adhesion, uptake, subcellular distribution, and cytotoxicity. The surface charge on CNPs can be engineered or modified to be positive, negative, or neutral by treatment with appropriate acidic/basic buffers or coating with a polymer, biomolecule, ligand, or surfactant/stabilizer. The surface charge of CNPs can be easily determined by measuring the zeta potential using a zeta potential analyzer. The zeta potential is the potential difference between dispersion medium and the stationary layer of fluid attached to the dispersed particles [140]. As a rule of thumb, a high zeta potential value above 30 mV or below −30 mV provides a stable dispersion (electric stabilization). However, for NPs made with high molecular weight polymers, surfactants or stabilizers, their suspension can be stable even at low zeta potential (steric stabilization). Thus, a minimum zeta potential of ±20 mV is desirable for the high stability of NPs possessing combined electrostatic and steric stabilization [141].

The uptake of NPs by cells usually involves two major steps a binding step on the cell membrane and an eventual internalization step. The first step is mainly affected by surface charge on both CNPs and cell membrane, with CNPs carrying higher surface charge being bound strongly to the cell membrane through electrostatic interaction [142]. Cell surfaces predominantly consist of negatively charged sulfated proteoglycans with their core proteins being anchored to the membrane and linked to one or more anionic glycosaminoglycans. Therefore, if the NPs are positively charged, their interaction with the cell surface will be predominantly through electrostatic forces. However, the negatively charged CNPs with zeta potential −43 mV were shown to possess higher cellular uptake than CNPs with a less negative or positive surface charge [111]. Although the

anionic cell membranes should repel negatively charged CNPs, it was suggested that the negatively charged CNPs can bind to specific cationic sites on the cell surface in the form of clusters. This localized neutralization can cause subsequent bending of the cell membrane, thereby facilitating cellular uptake by endocytosis. Patil et al. [111] and Renu et al. [53] also demonstrated preferential uptake of negatively charged CNPs by lung cancer cells A549 and prostate cancer cells PC-3, respectively. On the contrary, Vincent et al. [70] reported a higher uptake of positively charged transferrin-coated CNPs by A549 cells compared to that by normal WI-38 cells. In a review on the role of different NPs' surface charge on cytotoxicity, Frohlich [142] concluded that positively charged NPs are preferentially internalized by non-phagocytic cells, while negatively charged by phagocytic cells. Thus, apparently, the cellular uptake of differently surface-charged CNPs can vary depending on the cell type.

A careful monitoring of CNPs' surface charge is pivotal as it can switch from positive (kinetically stable state) to negative (thermodynamically stable state) following an increase in pH, time, temperature, and CNPs concentration through adsorption of $OH^-$ ions onto CNPs surface and thereby cause different cytotoxic effects. Vincent et al. [143] studied the change in surface charge upon varying the pH [3–14] of CNPs by using acidic and basic buffers and found no change in zeta potential for CNPs treated with acidic buffer (Figure 5(A)). However, for alkaline buffer-treated CNPs, a shift from positive to negative was observed following an increase in pH with the isoelectric point occurring at pH 10. Upon aging, the zeta potential of positively charged CNPs changed to negative after 40 days, while after 220 days both positively and negatively charge CNPs exhibited high negative zeta potential values ranging from −26 to −36 mV. The observed pH and time dependent shift from positive to negative zeta potential values was due to replacement of positively charged surface species on CNPs' surface ($H^+$) with negatively charged counterions ($OH^-$ ions) as shown in a schematic diagram (Figure 5(B)). Similar zeta potential shifts with increasing pH were also reported by Patil et al. [111] and Veriansyah et al. [144] for microemulsion/hydrothermal-based CNPs and decanoic acid/oleic acid-modified CNPs with the isoelectric point being at pH 4.5/9.5 and pH 7.5/8, respectively. Likewise, the zeta potential of both undoped and CNPs-doped with 20% yttrium (Y) or ytterbium (Yb) decreased following a rise in temperature with a surface charge shift at 65 °C (Figure 5(C)) [143]. At temperatures <50 °C, Y-doped CNPs exhibited a higher positive zeta potential and Yb-doped CNPs a lower positive zeta potential than undoped CNPs, with the zeta potential and oxygen vacancy defect concentration decreasing in the order: Y-CNPs > undoped CNPs > Yb-CNPs. Furthermore, following a raise in annealing temperature from 100 to 500 °C, the zeta potential value decreased from +43.0 to +1.65 mV, and with further elevation to 900 °C, a reversal of surface charge from positive to negative occurred (−20.6 mV), suggesting a faster rate of $OH^-$ adsorption at annealing temperatures caused by a reduction in oxygen vacancy defects, rate of $H_2O$ dissociation, and $H_3O^+$ production (Figure 5(D)). For the same reason, a gradual shift in surface charge from positive to negative also occurred with a decrease in concentration from 1 mM (+43.0 mV) to 10 μm (−24.1 mV), while the surface charge remained unaltered at >1 mM (Figure 5(E)).

Upon increasing the cerium oxide to micrometer size, a negative zeta potential value of −29.0 mV was obtained (Figure 5(D)). In addition, the interaction energy between CNPs and cell surface can affect cytotoxicity. In a comparative study dealing with seven metal oxide NPs, Li et al. [145] reported that the NPs possessing a lower interaction energy barrier with the cell surface could induce higher cytotoxicity by following the order: $Al_2O_3 < TiO_2 < CeO_2 < ZnO < SiO_2 < CuO < Fe_2O_3$ NPs, implying that the lower the energy barrier, the easier the adhesion to cell surface, and the higher the cytotoxicity. After internalization, the eventual localization of CNPs within cells is also dependent upon the CNPs' surface charge. For instance, both positively charged and neutral dextran-coated CNPs were shown to internalize in both normal cells (H9C2 and HEK293) and cancer cells (A549 and MCF-7) with the positive CNPs internalizing in both lysosome and cytoplasm causing cytotoxicity to all the cells except MCF-7, while the neutral CNPs in the cytoplasm showed no significant cytotoxicity [71]. However, the negatively charged ones exhibited cytotoxicity only towards lung cancer cell A549 mainly due to lysosomal localization.

More recently, it was widely reported that regardless of the surface charge on CNPs after synthesis, it could be changed to negative upon treatment with cell-culture medium, probably due to conjugation with protein or phosphate in the medium. In a study dealing with induction of angiogenesis by CNPs, Das et al. [91] showed that both positive CNPs (+44 mV) and negative CNPs (−20 mV) changed to negative (−9.23 mV) after treatment with endothelial basal media-2 containing 2% FBS. Also, Naganuma and Traversa [146] reported a shift of both positive CNPs (high $Ce^{3+}$) and negative CNPs (high $Ce^{4+}$) on poly-L-lactide acid scaffolds into negative after treatment with the Eagle's MEM medium containing 10% FBS, suggesting that protein-bound

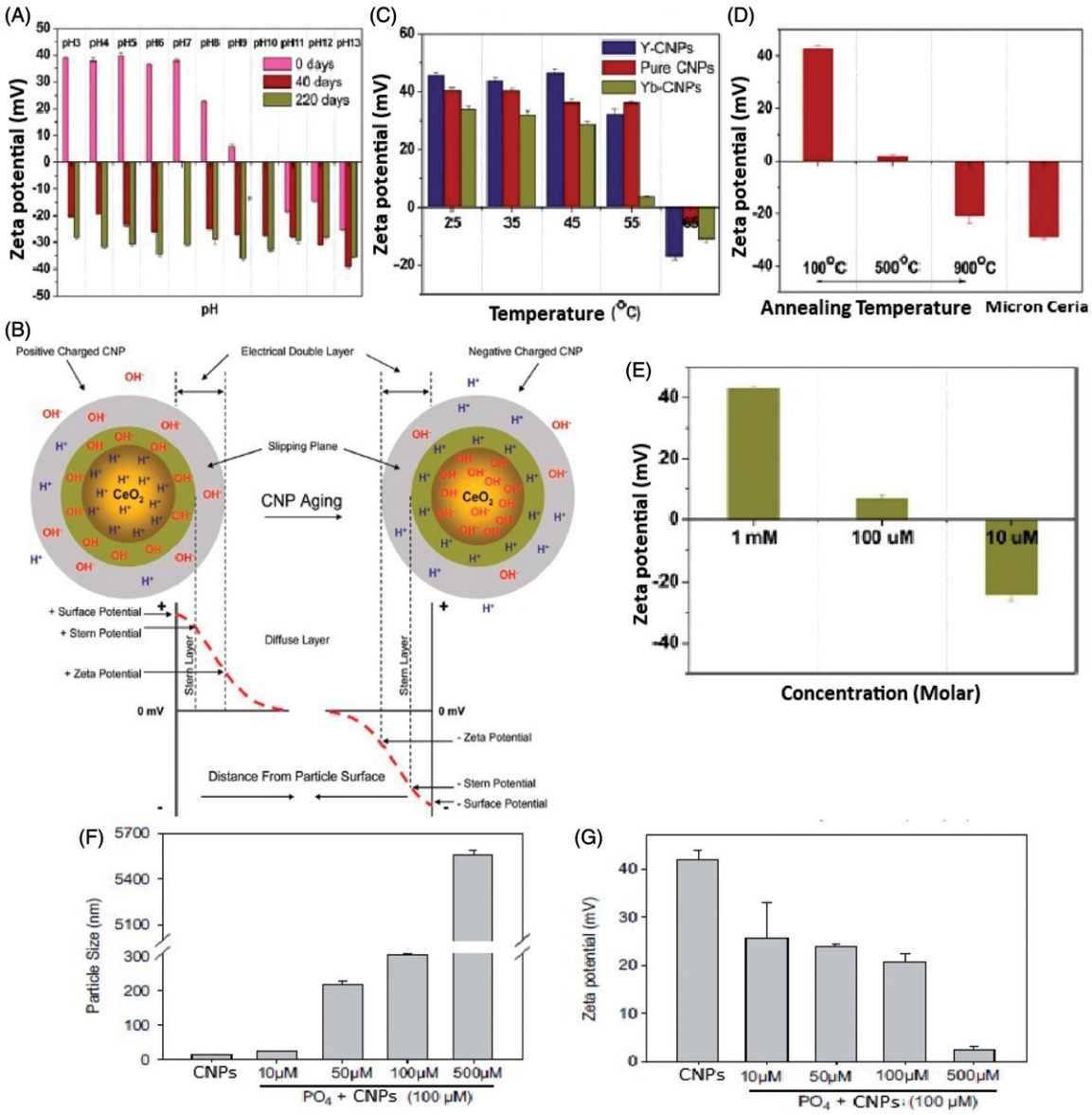


**Figure 5.** Effect of different pH buffers and aging time on zeta potential of CNPs at room temperature (A) with schematic diagram showing replacement of positively charged surface species ($H^+$) from CNPs' surface with the negatively charged counterions ($OH^-$) upon aging (B) as well as effect of temperature and doping (C), annealing temperature (D) and concentration (E) on zeta potential of CNPs. Effect of phosphate at different concentrations (10, 50, 100, and 500 μM) on particle size (F) and zeta potential (G) of CNPs. Doping of CNPs in (C) consists of 20% yttrium (Y) or ytterbium (Yb). (With permission from Vincent et al. [143] and Singh et al. [117]).

CNPs can entirely eliminate the electrostatic difference between the positively and negatively charged CNPs. Moreover, it was observed that a high level of $Ce^{4+}$ CNPs promoted proliferation of osteoblast cells MG63, while high $Ce^{3+}$ CNPs inhibited the growth of human mesenchymal stem cells MG63, demonstrating that the $Ce^{3+}/Ce^{4+}$ ratio on CNPs may contribute more to cytotoxicity than surface charge. But for interaction with proteins, some contradictory results were reported for positively or negatively charged CNPs. For instance, a highly positive CNP surface could favor more adsorption of transferrin protein, resulting in better cell adhesion via ligand–receptor mediated interactions [70]. Whereas, in another study, although positively charged CNPs could adsorb more bovine serum albumin (BSA), a higher uptake in A549 cells was shown only for negatively charged CNPs with poor protein adsorption capacity [111]. Interestingly, a different phenomenon was observed by Naganuma and Traversa [146], reporting no significant difference in BSA adsorption between positively and negatively charged CNPs with adsorbed BSA being unassociated with inhibition of cell adhesion and proliferation of MG63 and hMSCs cells. Nevertheless, the effect due to interaction with other

proteins or components cannot be ignored. This is because the CNPs can interact with numerous biomolecules especially proteins and attain a new biological identity when they come in contact with the biological environment (please refer to biological identity in the Supplementary Information).

In the presence of a biologically important phosphate buffer, an increase in particle size and a drop in zeta potential was shown to occur [117]. More elaborately, by increasing the phosphate concentration from 10 to 100 μM, the particle size of CNPs increased from 24 to 290 nm with a stable suspension (Figure 5(F)). Likewise, a drop in zeta potential occurred with an increase in phosphate concentration (Figure 5(G)), which may be due to electrostatic attraction between phosphate anions and positive charge on CNPs surface resulting in charge neutralization. However, a further increase in phosphate level to 500 μM resulted in precipitation with an average aggregate size of ∼5500 nm.

Taken together, the effect of CNPs' surface charge on cytotoxicity revealed their tendency to turn negative following changes in pH, temperature, time (aging), concentration, and doping as well as interaction with proteins in cell culture medium. Also, a decrease in zeta potential was observed upon treatment with a biological buffer containing phosphate. Therefore, a careful monitoring of change in surface charge during storage as well as before and after treatment with cell-culture medium is important. In other words, both qualitative and quantitative analyses of type and level of protein binding as well as conjugation of cell-culture/biological buffer components on CNPs surface should be carried out.

## Cellular uptake and sub-cellular localization

Cellular uptake, a key biomarker for evaluating the cytotoxicity of any nanoparticle, is often determined by flow cytometry or ICP-MS techniques. The former involves measurement of increase in side-scattering due to accumulation of CNPs inside the cells, while the latter is based on direct quantitation of CNPs inside the cell through the cerium metal ion concentration [142,147]. For sub-cellular localization, both high-resolution TEM and fluorescence imaging techniques are widely used to precisely monitor the distribution of CNPs in different microcomparments inside the cell [147]. After initial CNPs-cell interaction and attachment through surface charge, the CNPs can enter into cells through several pathways, such as phagocytosis and receptor-mediated endocytosis/pinocytosis, with the latter being further classified into: macropinocytosis, clathrin-mediated endocytosis, caveolae-mediated endocytosis, and clathrin/caveolae-independent endocytosis [142,148]. Once internalized, CNPs are further sorted and trafficked to different organelles inside the cell. Accordingly, the CNPs can be localized into mitochondria, lysosome, endoplasmic reticulum, cytoplasm, and nucleus for imparting protective or cytotoxic effects [2]. Hirst et al. [31] reported two CNPs of different size (3–5 and 10–50 nm in the dry state) to be engulfed by phagocytosis and localized in both phagosomes and cytosol of murine macrophage cells J774A.1. Conversely, in a study dealing with the elucidation of cytotoxicity mechanism of CNPs towards human keratinocyte cell HaCat, Singh et al. [148] found rapid uptake of carboxy-fluorescence conjugated CNPs (CCNPs) within 3 h through energy-dependent, clathrin-mediated and caveolae-mediated endocytic pathways, by disrupting the main energy source ATP using $NaN_3$ and 2-deoxy-D-glucose or formation of clathrin-coated pits using $K^+$ ion depleted buffer/hypertonic sucrose or formation of cholesterol-rich caveolae using methyl-beta-cyclodextrin (MβCD)/nystatin, with the uptake of CCNPs being substantially reduced compared to control (Supplementary Figure S2). A similar uptake mechanism in human endothelial HUVEC cell EA.hy926 and localization into cytoplasm was reported by Chen et al. [149], demonstrating the protective action of CNPs against oxidative stress-induced apoptosis. For cellular uptake and suppression of ROS in mouse macrophage RAW264.7 cells, Zhou et al. [150] used ICP-MS to demonstrate the internalization of two commercial CNPs (D-$CeO_2$ and PC-$CeO_2$) and found that the cellular uptake increased following a rise in the CNPs dose and incubation time, with the latter CNPs showing faster uptake rates and higher cellular loading at 200 μg/mL. Based on the blocking of macropinocytosis by amiloride-HCl, clathrin-mediated endocytosis by amantadine-HCl, and caveolae-mediated endocytosis by genistein, the internalization of D-$CeO_2$ was reported to predominantly occur through macropinocytosis, while PC-$CeO_2$ accumulated through caveolae-mediated endocytosis. Nevertheless, clathrin-mediated endocytosis also played a vital role in cellular uptake of both CNPs [150].

Several studies have shown size-, shape-, oxidation state-, treatment time-, dose-, coating-, and cell type-dependent cellular uptake mechanisms, internalization efficiency, and sub-cellular localization. Vassie et al. [151] have shown both colon cancer cells HT-29 and ovarian cancer cells SKOV3 to internalize 7 nm or 94 nm FITC-conjugated CNPs through clathrin and caveolin-1 endocytosis, respectively, with the internalization of 94 nm CNPs into ovarian cell lysosomes being more than 7 nm CNPs (Supplementary Figure S2). However, no size-dependent uptake was found in colon cancer

cells treated with FITC-CNPs. In addition, compared to 24 h incubation, the uptake of 7 nm and 94 nm FITC-CNPs by ovarian cancer cells was greater after 1 h and 4 h incubation, respectively, while an opposite trend was observed for colon cancer cells as the level of 7 nm or 94 nm FITC-CNPs internalized into lysosomes was higher for 24 h incubation, demonstrating a time-dependent response for CNPs uptake by cancer cells (Supplementary Figure S2).

Recently, a shape-dependent cellular uptake of CNPs was studied by Mahapatra et al. [137], illustrating a faster cellular uptake rate of cerium oxide nanospheres (CNPs), small-sized nanorods (s-CNRs), and medium-sized nanorods (m-CNRs) by human dental stem (HDS) cells than highly elongated nanowires (CNWs). During the initial treatment phase, the CNWs were found in the extracellular space, while CNPs, s-CNRs and m-CNRs were located primarily in the intracellular compartment, facilitating ROS scavenging in both extracellular and intracellular sites of HDS cells. However, the internalization of CNWs can also be increased after 48 h and 72 h treatment. Moreover, the CNPs were internalized through clathrin- and caveolae-mediated endocytic pathways and localized in endosomes, while CNWs were located within lysosome and cytosol organelles. Several rod-type nanomaterials with high aspect ratios have been reported to possess the capability to spontaneously enter the cells [152,153]. However, nanowires or nanotubes, due to excessive high axial dimension (above 500 nm), may require more time and energy to undergo cell internalization, thereby limiting their uptake rate [137]. Nevertheless, the nanowires, which are oriented perpendicular to the plasma membrane, were engulfed by cells through perforation and diffusion of a lipid bilayer without causing cell death [154].

The oxidation state of CNPs can also play a key role in dictating the cellular uptake as evidenced by several recent studies. In a study dealing with poly-L-lactide scaffold functionalized with layers of CNPs, the regions with dominant $Ce^{4+}$ were shown to be more favorable than $Ce^{3+}$ regions for the uptake by human mesenchymal stem cells [146]. Based on this phenomenon, Vassie et al. [151] also pointed out that $Ce^{4+}$ dominant CNPs (74%) possessed superior internalization efficiency over CNRs and CNWs ($Ce^{4+} = 25–40\%$) for HDS cells. Moreover, a shift to a higher $Ce^{3+}/Ce^{4+}$ ratio was found in CNPs internalized within mouse alveolar II epithelial cells (C10) compared to those outside the cell, with the ratio being similar in both cytoplasm and lysosome [155]. A dose-dependent cellular uptake and intracellular ROS scavenging was reported by Zhang et al. [156], who observed a variation in side-scatter intensity (375–620%) compared to control (100%) for cellular uptake of both 25 nm and 50 nm CNPs by bone marrow stromal cells (BMSCs). These authors have also demonstrated a synergistic multiple endocytosis mechanism with a combination of macropinocytosis, clathrin, and caveolae mediated endocytic processes.

For sub-cellular localization, Zhang et al. [156] showed the distribution of CNPs in the cytoplasm of BMSCs, but failed to enter the nucleus. Similar results were reported in several other studies, for instance, Babu et al. [157] visualized a predominant localization of CNPs by TEM, with Au-decorated CNPs (~10 nm in dry state) located in both the cytoplasm and lysosome of lung cancer cells A549, but not in the nucleus. It is possible that the CNPs size may increase in cell-culture medium surpassing the critical size of nuclear pores. In a similar study, Zhou et al. [147] reported that the size of two commercial CNPs with 20 nm and 8 nm could increase to 190 nm and 60 nm, respectively, in cell-culture medium, thereby being unable to enter the nucleus. Conversely, Singh et al. [148] observed CCNPs localized in the cytoplasm and nucleus as shown by photoluminescence spectra of whole cell, cytoplasmic and nuclear extracts, as well as in mitochondria, lysosomes and endoplasmic reticulum (Supplementary Figure S3). As the diameter of a mammalian nuclear pore complex is approximately 120 nm, the actual diameter of pore that allows inert molecules like nanoparticles to enter is only 9 nm and may further dilate to 26 nm upon internalization [148,158]. Thus, the CNPs may enter the nucleus if CNPs are present as individual particles or small aggregates inside the cells, but not as complex clusters.

Functionalization and/or surface-bound chemicals such as ions, lipids, and proteins on CNPs can significantly alter the efficiency and mechanism of cellular uptake as well as cytotoxicity. For example, Vincent et al. [70] demonstrated higher uptake of transferrin-coated CNPs by A549 cells through receptor-mediated endocytosis compared to bare CNPs. Likewise, a 2-fold higher cellular uptake was reported for hexamethylenetetramine-coated CNPs when compared to bare CNPs, implying that the presence of a functional group/stabilizer can improve CNPs-cell interaction and eventual uptake as well as cytotoxicity [11]. Ting et al. [159] also reported more effective internalization of heparin-functionalized CNPs and the scavenging of ROS in both non-activated U937 and phorbol 12-myristate 13-acetate activated U937cells within 24 h in a dose-dependent manner than bare CNPs. Functionalization can also facilitate entry of CNPs into different sub-cellular micro-compartments to impose protective or cytotoxic effects. Lord et al. [160,161] have shown bare CNPs to be internalized within the cytoplasm of human fetal lung

fibroblast cells MRC5 and primary human coronary artery endothelial cells (HCAEC), respectively, while heparin-coated and hyaluronan-coated CNPs were localized in both cytoplasm and lysosome with the heparin-coated CNPs exhibiting ROS scavenging activity in cytoplasm and oxidase activity in lysosomes. Similarly, β-cyclodextrin-coated and dextran-coated CNPs were shown to internalize inside the acidic lysosome environment [162,163]. However, polymer-coated CNPs may show a different phenomenon depending upon cell type. For example, dextran-coated CNPs were reported to internalize within the lysosome of human embryonic kidney cells HEK293 and cardiac myocyte cells H9c2, but not within breast cancer cells MCF-7 and lung cancer cells A549 [71]. On the other hand, poly(3-sulfopropylmatheacrylate)- and poly (2-metharyloyloxy)ethyl-trimethylammonium chloride)-coated CNPs were internalized within endosomes, lysosomes and lipid bodies in high proportions compared to bare CNPs [164]. Some polymer-coated CNPs were also reported to induce lysosome-autophagy systems, the main catabolic pathway activated in mammalian cells by exogenous materials. Song et al. [165] functionalized CNPs with different biocompatible coatings including N-acetylglucosamine, polyethylene glycol, and polyvinylpyrrolidone, and demonstrated that these CNPs could activate a master regulator of lysosome function and autophagy transcription factor EB, induce upregulation of lysosome-autophagy system genes and promote clearance of toxic aggregates in cells possessing an inefficient lysosomal system. Similarly, in another report, Lord et al. [161] further illustrated that hyaluronan-coated CNPs after internalization into human fetal lung fibroblast cells MRC5 through a CD44-mediated process were localized in lysosome and induced autophagy.

In addition, the difference in the level of cellular uptake and intracellular localization for the same CNPs can depend upon the cell type. Asati et al. [71] reported higher uptake of aminated polyacrylic acid-coated CNPs (ANCs) by human embryonic kidney cells HEK293 than by cardiac myocytes cell (H9c2). Also, among various cancer cells, the lung cancer cell A549 internalized more ANCs than the breast cancer cell MCF-7. For polyacrylic acid-coated CNPs (PNCs), A549 cells showed a higher degree of uptake than HEK293 cells, implying a difference in cellular uptake between normal cells and cancer cells. More recently, upon incubation with 94 nm FITC-CNPs, the ovarian cancer cell SKOV3 was shown to uptake more CNPs after 4 h compared to colon cancer cell HT-29, while a reversed order was found after 24 h (Supplementary Figure S2) [151].

Overall, the internalization of CNPs by cells was shown to be: size-, shape-, time-, dose-, coating-, and oxidation state-dependent with the cellular uptake predominantly occurring through endocytosis. Functionalization of CNPs favored high cellular uptake and subcellular localization depending upon cell type and physicochemical properties of CNPs.

## Summary

Although the unique redox capability of CNPs has promising biological applications, there are still several issues needed to be elucidated for possible future clinical translation into a practical drug. The controversial outcomes of antioxidant or pro-oxidant effects of CNPs is largely attributed to differences in synthesis methods and physicochemical characteristics. Moreover, the CNPs' size, shape, oxidation state, and surface charge can significantly influence their cellular attachment, uptake efficiency, uptake mechanism, and distribution in different microenvironments, thereby generating variable cytotoxic effects. However, based on this review, it is difficult to establish solid trends relating CNPs physicochemical properties with biological activity as contrasting results have been reported in the literature. This can partly be remedied by a careful and complete characterization of synthesized CNPs along with detailed description of a synthesis protocol, processing, storage and handling conditions, all of which can be the possible determinants of their biological efficiency. In addition, a complete characterization of *in vitro* conditions such as medium pH, protein and salt concentration should be carried out. Characterization of CNPs should also be performed at every stage of their application both intermittently and finally during *in vitro*/in vivo tests for better elucidation of toxicity variation. Given the large diversity in variety and abundance of biomolecules especially proteins, it is imperative to elucidate the nature of CNPs-protein interactions for assessing their biological efficiency. Strategies to improve dispersion, reduce agglomeration, and lower protein interaction including coating with appropriate biocompatible and biodegradable organic compounds should be devised without compromising their biological effects. On the other hand, studies should also be carried out to unravel the effects of different cell types and cell surface characteristics on cytotoxicity of CNPs. Collaborative studies between different research groups should be carried out for overcoming issues of difference in synthesis as affected by experimental conditions. Thus, a rigorous task lies ahead for a better understanding of CNPs' physical and chemical properties as well as their complex interactions with

biological systems as this is critical for CNPs to attain a clinical drug status.

## Disclosure statement

There is no conflict of interest to declare by the authors.

## References


[1] Jukupec MA, Unfried P, Keppler BK. Pharmacological properties of cerium compounds. Rev Physiol Biochem. 2005;153:101–111.

[2] Nelson BC, Johnson ME, Walker ML, et al. Antioxidant cerium oxide nanoparticles in biology and medicine. Antoxidants. 2016;5:E15.

[3] Esch F, Fabris S, Zhou L, et al. Electron localization determines defect formation on ceria substrates. Science. 2005;309:752–755.

[4] Tsai YY, Oca-Cossio J, Lin SM, et al. Reactive oxygen species scavenging properties for $ZrO_2$-$CeO_2$ solid solution nanoparticles. Nanomedicine. 2008;3: 637–645.

[5] Fronzi M, Soon A, Delley B, et al. Stability and morphology of cerium oxide surfaces in an oxidizing environment: a first-principles investigation. J Chem Phys. . 2009;131:104701.

[6] Deshpande S, Patil S, Kuchibhatia SVNT, et al. Size dependency variation in lattice parameter and valency states in nanocrystalline cerium oxide. Appl Phys Lett. 2005;87:133113.

[7] Celardo I, Pedersen JZ, Traversa E, et al. Pharmacological potential of cerium oxide nanoparticles. Nanoscale. 2011;3:1411–1420.

[8] Fukui K, Namai Y, Iwasawa Y. Imaging of surface oxygen atoms and their defect structures on $CeO_2$(111) by noncontact atomic force microscopy. Appl Surf Sci. 2002;188:252–256.

[9] Namai Y, Fukui K, Iwasawa Y. Atom-resolved noncontact atomic force microscopic observations of $CeO_2$ (111) surfaces with different oxidation states: surface structure and behavior of surface oxygen atoms. J Phys Chem B. 2003;107:11666–11673.

[10] Karokoti A, Singh S, Dowding JM, et al. Redox-active radical scavenging nanomaterials. Chem Soc Rev. 2010;39:4422–4432.

[11] Dowding JM, Das S, Kumar A, et al. Cellular interaction and toxicity depend on physicochemical properties and surface modification of redox-active nanomaterials. ACS Nano. 2013;7:4855–4868.

[12] Zheng X, Zhang X, Wang X, et al. Preparation and characterization of $CuO/CeO_2$ catalysis and their applications in low-temperature CO oxidation. Appl Catal A. 2005;295:142–149.

[13] Yamashita M, Kameyama K, Yabe S, et al. Synthesis and microstructure of calcia doped ceria as UV filters. J Mater Sci. 2002;37:683–687.

[14] Corma A, Atienzar P, Garcia H, et al. Hierarchically mesostructured doped CeO2 with potential for solar-cell use. Nat Mater. 2004;3:394–397.

[15] Murray EP, Tsai T, Barnett SAA. Direct methane fuel cell with a ceria-based anode. Nature. 1999;400: 649–651.

[16] Esposito V, Traversa E. Design of electroceramics for solid oxide fuel cell applications: playing with ceria. J Am Ceram Soc. 2008;91:1037–1051.

[17] Izu N, Shin W, Matsubara I, et al. Development of resistive oxygen sensors based on cerium oxide thick film. J Electroceram. 2004;13:703–706.

[18] Korsvik C, Patil S, Seal S, et al. Superoxide dismutase mimetic properties exhibited by vacancy engineered ceria nanoparticles. Chem Commun. 2007;10: 1056–1058.

[19] Pirmohamed T, Dowding JM, Singh S, et al. Nanoceria exhibit redox state-dependent catalase mimetic activity. Chem Commun. 2010;46:2736–2738.

[20] Xue Y, Luan Q, Yang D, et al. Direct evidence for hydroxyl radial scavenging activity of cerium oxide nanoparticles. J Phys Chem C. 2011;115:4433–4438.

[21] Dowding JM, Dosani T, Kumar A, et al. Cerium oxide nanoparticles scavenge nitric oxide radical (NO). Chem Commun (Camb). 2012;48:4896–4898.

[22] Singh N, Cohen CA, Rzigalinski BA. Treatment of neurogenerative disorders with radical nanomedicine. Ann N Y Acad Sci. 2007;1122:219–230.

[23] Rzigalinski BA, Carfagna CS, Ehrich M. Cerium oxide nanoparticles in neuroprotection and considerations for efficacy and safety. WIREs Nanomed Nanobiotechnol. 2017;9:e1444.

[24] D'Angelo B, Santucci S, Benedetti E, et al. Cerium oxide nanopartcles triger neuronal survical in a human Alzheimer disease model by modulating BDNF pathway. Curr Nanosci. 2009;5:167–176.

[25] Kim CK, Kim T, Choi IY, et al. Nanoparticles that can protect against ischemic stroke. Angew Chem Int Ed Engl. 2012;124:11201–11205.

[26] Niu J, Azfer A, Rogers LM, et al. Cardioprotective effects of cerium oxide nanoparticles in a transgenic murine model of cardiomyopathy. Cardiovasc Res. 2007;73:549–559.

[27] Selvaraj V, Manne ND, Arvapalli R, et al. Effect of cerium oxide nanoparticles on sepsis induced mortality and NF-κB signaling in cultured macrophages. Nanomedicine. 2015;10:1275–1288.

[28] Pourkhalili N, Hosseini A, Nili-Ahmadabadi A, et al. Biochemical and cellular evidence of the benefit of a combination of cerium oxide nanoparticles and selenium to diabetic rats. World J Diabetes. 2011;2: 204–210.

[29] Chen JP, Patil S, Seal S, et al. Rare earth nanoparticles prevent retinal degeneration induced by intracellular peroxides. Nat Nanotechnol. 2006;1:142–150.

[30] Zhou XH, Wong LL, Karakoti AS, et al. Nanoceria inhibit the development and promote the regression of pathogenic retinal neovascularization in the vldlr knockout mouse. PLoS One. 2011;6:e16733.

[31] Hirst SM, Karakoti AS, Tyler RD, et al. Anti-inflammatory properties of cerium oxide nanoparticles. Small. 2009;5:2848–2856.

[32] Lin W, Huang YW, Zhou XD, et al. Toxicity of cerium oxide nanoparticles in human lung cancer cells. Int J Toxicol. 2006;25:451–457.

[33] Alili L, Sack M, Karakoti AS, et al. Combined cytotoxic and anti-invasive properties of redox-active nanoparticles in tumor-stroma interactions. Biomaterials. 2011;32:2918–2929.

[34] Celardo I, De Nicola M, Mandoli C, et al. $Ce^{3+}$ ions determine redox-dependent anti-apoptotic effect of cerium oxide nanoparticles. ACS Nano. 2011;5: 4537–4549.

[35] Sharpe E, Andreescu D, Andreescu S. Artificial nanoparticle antioxidants. In: Andreescu S, Hepel M, editors. Oxidative stress: diagnostics, prevention, and therapy. Washington (DC): American Chemical Society; 2011. p. 235–253.

[36] Estevez AY, Erlichman JS. The potential of cerium oxide nanoparticles (nanoceria) for neurodegenerative disease therapy. Nanomedicine (Lond). 2014;9: 1437–1440.

[37] Das S, Dowding JM, Klump KE, et al. Cerium oxide nanoparticles: applications and prospects in nanomedicine. Nanomedicine (Lond). 2013;8:1483–1508.

[38] Xu C, Qu X. Cerium oxide nanoparticle: a remarkably versatile rare earth nanomaterial for biological applications. NPG Asia Mater. 2014;6:e90.

[39] Ganesana M, Erlichman JS, Andreescu S. Real-time monitoring of superoxide accumulation and antioxidant activity in a brain slice model using an electrochemical cytochrome c biosensor. Free Radic Biol Med. 2012;53:2240–2249.

[40] Tarnuzzer RW, Colon J, Patil S, et al. Vacancy engineered ceria nanostructures for protection from radiation-induced cellular damage. Nano Lett. 2005;5:2573–2577.

[41] Colon J, Hsieh N, Ferguson A, et al. Cerium oxide nanoparticles protect gastrointestinal epithelium from radiation-induced damage by reduction of reactive oxygen species and upregulation of superoxide dismutase 2. Nanomedicine. 2010;6:698–705.

[42] Eom HJ, Choi J. Oxidative stress of $CeO_2$ nanoparticles via p38-Nrf-2 signaling pathway in human bronchial epithelial cell, Beas-2B. Toxicol Lett. 2009;187:77–83.

[43] Auffan M, Rose J, Orsiere T, et al. $CeO_2$ nanoparticles induce DNA damage towards human dermal fibroblasts in vitro. Nanotoxicology. 2009;3:161–171.

[44] Yokel RA, Florence RL, Unrine JM, et al. Biodistribution and oxidative stress effects of a systemically-introduced commercial ceria engineered nanomaterial. Nanotoxicology. 2009;3:234–248.

[45] Ma JY, Zhao H, Mercer RR, et al. Cerium oxide nanoparticles-induced pulmonary inflammation and alveolar macrophage functional change in rats. Nanotoxicology. 2011;5:312–325.

[46] Srinivas A, Rao PJ, Selvam G, et al. Acute inhalation toxicity of cerium oxide nanoparticles in rats. Toxicol Lett. 2011;5:105–115.

[47] Zhang HFZ, He XA, Zhang ZY, et al. Nano-$CeO_2$ exhibits adverse effects at environmental relevant concentrations. Environ Sci Technol. 2011;45: 3725–3730.

[48] Hussain S, Al-Nsour F, Rice AB, et al. Cerium dioxide nanoparticles induce apoptosis and autophagy in human peripheral blood monocytes. ACS Nano. 2012;6:5820–5829.

[49] Thill A, Zeyons O, Spalla O, et al. Cytotoxicity of $CeO_2$ nanoparticles for *Escherichia coli*. physico-chemical insight of the cytotoxicity mechanism. Environ Sci Technol. 2006;40:6151–6156.

[50] Hardas SS, Butterfield DA, Sultana R, et al. Brain distribution and toxicological evaluation of a systemically delivered engineered nanoscale ceria. Toxicol Sci. 2010;116:562–576.

[51] Pierscionek BK, Keenan J, Yasseen A, et al. $CeO_2$ nanoparticles have no detrimental effect on eye lens proteins. Curr Anal Chem. 2010;6:172–176.

[52] Babu S, Cho J, Dowding JM, et al. Multicolored redox active upconverter cerium oxide nanoparticle for bioimaging and therapeutics. Chem Commun. 2010; 46:6915–6917.

[53] Renu G, Rani VVD, Nair SV, et al. Development of cerium oxide nanoparticles and its cytotoxicity in prostate cancer cells. Adv Sci Lett. 2012;6:17–25.

[54] Asati A, Santra S, Kaittanis C, et al. Oxidase-like activity of polymer-coated cerium oxide nanoparticles. Angew Chem Int Ed Engl. 2009;48:2308–2314.

[55] Cedervall T, Lynch I, Lindman S, et al. Understanding the nanoparticle-protein corona using methods to quantify exchange rates and affinities of proteins for nanoparticles. Proc Natl Acad Sci USA. 2007;104: 2050–2055.

[56] Karmali PP, Simberg D. Interactions of nanoparticles with plasma proteins: implication on clearance and toxicity of drug delivery systems. Expert Opin Drug Deliv. 2011;8:343–357.

[57] Hu Z, Haneklaus S, Sparovek G, et al. Rare earth elements in soils. Commun Soil Sci Plant Anal. 2006;37:1381–1420.

[58] Suzuki T, Kosacki I, Anderson HU, et al. Electrical conductivity and lattice defects in nanocrystalline cerium oxide thin films. J Am Ceram Soc. 2001;84: 2007–2014.

[59] Zhang F, Chen CH, Raitano JM, et al. Phase stability in ceria zirconia binary oxide nanoparticles: the effect of the $Ce^{3+}$ concentrations and the redox environment. J Appl Phys. 2006;99:084313.

[60] Schwarz K. Materials design of solid electrolytes. Proc Natl Acad Sci USA. 2006;103:3497.

[61] Kuchma MH, Komanski CB, Colon J, et al. Phosphate ester hydrolysis of biologically relevant molecules by cerium oxide nanoparticles. Nanomed Nanotechnol. 2010;6:738–744.

[62] Dutta P, Pal S, Seehra MS, et al. Concentration of $Ce^{3+}$ and oxygen vacancies in cerium oxide nanoparticles. Chem Mater. 2006;18:5144–5146.

[63] Xiong F, Zhou D, Xie Z, et al. A study of the $Ce^{3+}$/$Ce^{4+}$ redox couple in sulfamic acid for redox battery application. Appl Energy. 2012;99:291–296.

[64] Heckert EG, Karakoti AS, Seal S, et al. The role of cerium redox state in the SOD mimetic activity of nanoceria. Biomaterials. 2008;29:2705–2709. 2008

[65] Skorodumova NV, Simak SI, Lundqvist BI, et al. Quantum origin of the oxygen storage capability of ceria. Phys Rev Lett. 2002;89:166601.

[66] Romeo M, Bak K, Elfallah J, et al. XPS study of the reduction of cerium dioxide. Surf Interface Anal. 1993;20:508–512.
[67] Binet C, Daturi M, Lavalley JC. IR study of polycrystalline ceria properties in oxidized and reduced states. Catal Today. 1999;50:207–225.
[68] Xia T, Kovochich M, Liong M, et al. Comparison of the mechanism of toxicity of zinc oxide and cerium oxide nanoparticles based on dissolution and oxidative stress properties. ACS Nano. 2008;2:2121–2134.
[69] Demokritou P, Gass S, Pyrgiotakis G, et al. An in vivo and in vitro toxicological characterisation of realistic nanoscale $CeO_2$ inhalation exposures. Nanotoxicology. 2013;7:1338–1350.
[70] Vincent A, Babu S, Heckert E, et al. Protonated nanoparticle surface governing ligand tethering and cellular targeting. ACS Nano. 2009;3:1203–1211.
[71] Asati A, Santra S, Kaittanis C, et al. Surface-charge-dependent cell localization and cytotoxicity of cerium oxide nanoparticles. ACS Nano. 2010;4:5321–5331.
[72] Tseng MT, Lu X, Duan X, et al. Alteration of hepatic structure and oxidative stress induced by intravenous nanoceria. Toxicol Appl Pharmacol. 2012;260:173–182.
[73] De Marzi L, Monaco A, De Lapuente J, et al. Cytotoxicity and genotoxicity of ceria nanoparticles on different cell lines in vitro. Int J Mol Sci. 2013;14:3065–3077.
[74] Schubert D, Dragusch R, Raitano J, et al. Cerium and yttrium oxide nanoparticles are neuroprotective. Biochem Biophys Res Commun. 2006;342:86–91.
[75] Wang X, Zhang D, Li Y, et al. Self-doped $Ce^{3+}$ enhanced $CeO_2$ host matrix for energy transfer from $Ce^{3+}$ to $Tb^{3+}$. RSC Adv. 2013;3:3623–3630.
[76] Laberty-Robert C, Long JW, Lucas EM, et al. Sol-gel derived ceria nanoarchitechures: synthesis, characterization, and electrical properties. Chem Mater. 2006;18:50–58.
[77] Ozer N. Optical properties and electrochromic characterization of sol-gel deposited ceria films. Sol Energy Mater Sol Cells. 2011;68:391–400.
[78] Dan M, Tseng MT, Wu P, et al. Brain microvascular endothelial cell association and distribution of a 5 nm ceria engineered nanomaterial. Int J Nanomedicine. 2012;7:4023–4036.
[79] Yokel RA, Tseng MT, Dan M, et al. Biodistribution and biopersistence of ceria engineered nanomaterials: size dependence. Nanomedicine. 2012;9:398–407.
[80] Cimini A, D'Angelo B, Das S, et al. Antibody-conjugated PEGylated cerium oxide nanoparticles for specific targeting of Aβ aggregates modulate neuronal survival pathways. Acta Biomater. 2012;8:2056–2067.
[81] Chaudhury K, Babu NK, Das S, et al. Mitigation of endometriosis using regenerative cerium oxide nanoparticles. Nanomedicine. 2013;9:439–448.
[82] Kamruddin M, Ajikumar PK, Nithya R, et al. Synthesis of nanocrystalline ceria by thermal decomposition and soft-chemistry methods. Scrip Mater. 2004;50:417–422.
[83] Guilou N, Nistor LC, Fuess H, et al. Microstructural studies of nanocrystalline $CeO_2$ produced by gas condensation. Nanostruct Mater. 1997;8:545–557.
[84] Yin L, Wang Y, Pang G, et al. Sonochemical synthesis of cerium oxide nanoparticles-effect of additives and quantum size effect. J Colloid Interf Sci. 2002;246:78–84.
[85] Zhou Y, Phillips RJ, Switzer JA. Electrochemical synthesis and sintering of nanocrystalline cerium(IV) oxide powders. J Am Ceram Soc. 1995;78:891–985.
[86] Lee SM, Cho SN, Cheon J. Anisotropic shape control of colloidal inorganic nanocrystals. Adv Mater. 2003;5:441–444.
[87] Burda C, Chen X, Narayanan R, et al. Chemistry and properties of nanocrystals of different shapes. Chem Rev. 2005;105:1025–1102.
[88] Gupta A, Das S, Neal CJ, et al. Controlling the surface chemistry of cerium oxide nanoparticles for biological application. J Mater Chem B. 2016;B4:3195–3202.
[89] Sun C, Li H, Chen L. Nanostructured ceria-based materials: synthesis, properties, and applications. Energy Environ Sci. 2012;5:8475–8505.
[90] Zhang D, Du X, Shi L, et al. Shape-controlled synthesis and catalytic application of ceria nanomaterials. Dalton Trans. 2012;41:14455–14475.
[91] Das S, Singh S, Dowding JM, et al. The induction of angiogenesis by cerium oxide nanoparticles through the modulation of oxygen in intracellular environments. Biomaterials. 2012;33:7746–7755.
[92] Karakoti AS, Kuchibhatla SVNT, Baer DR, et al. Self-assembly of cerium oxide nanostructures in ice molds. Small. 2008;4:1210–1216.
[93] Zhang F, Jin Q, Chan SW. Ceria nanoparticles: size, size distribution, and shape. J Appl Phys. 2004;95:4319–4326.
[94] Merrifield RC, Wang ZW, Palmer RE, et al. Synthesis and characterization of polyvinylpyrrolidone coated cerium oxide nanoparticles. Environ Sci Technol. 2013;47:12426–12433.
[95] Karakoti AS, Munusamy P, Hostetler K, et al. Preparation and characterization challenges to understanding environmental and biological impacts of nanoparticles. Surf Interface Anal. 2012;44:882–889.
[96] Mai HX, Sun LD, Zhang YW, et al. Shape-selective synthesis and oxygen storage behavior of ceria nanopolyhedra, nanorods, and nanocubes. J Phys Chem B. 2006;109:24380–24385.
[97] Zhou KB, Wang X, Sun XM, et al. Enhanced catalytic activity of ceria nanorods from well-defined reactive crystal planes. J Catal. 2005;229:206–212.
[98] Yang SW, Gao L. Controlled synthesis and self-assembly of $CeO_2$ nanocubes. J Am Chem Soc. 2006;128:9330–9331.
[99] Rogers NJ, Franklin NM, Apte SC, et al. Physico-chemical behavior and algal toxicity of nanoparticulate $CeO_2$ in fresh water. Environ Chem. 2010;7:50–60.
[100] Ji Z, Wang X, Zhang H, et al. Designed synthesis of $CeO_2$ nanorods and nanowires for studying toxicological effects of high aspect ratio nanomaterials. ACS Nano. 2012;6:5366–5380.
[101] Lin S, Wang X, Ji Z, et al. Aspect ratio plays a role in the hazard potential of $CeO_2$ nanoparticles in mouse lung and zebra fish. ACS Nano. 2014;8:4450–4464.

[102] Naganuma T. Shape design of cerium oxide nanoparticles for enhancement of enzyme mimetic activity in therapeutic applications. Nano Res. 2017;10:199–217.
[103] Hirano M, Kato E. Hydrothermal synthesis of cerium(IV) oxide. J Am Ceram Soc. 1996;79:777–780.
[104] Pan CS, Zhang DS, Shi LY, et al. Template-free synthesis, controlled conversion, and co-oxidation properties of $CeO_2$ nanorods, nanowires, and nanocubes. Eur J Inorg Chem. 2008;2008:2429–2436.
[105] Wu Q, Zhang F, Xiao P, et al. Great influence of anions for controllable synthesis of $CeO_2$ nanostructures: from nanorods to nanocubes. J Phys Chem C. 2008;112:17076–17080.
[106] Alili L, Sack M, von Montfort C, et al. Downregulation of tumor growth and invasion by redox-active nanoparticles. Antioxid Redox Signal. 2013;19:765–778.
[107] Perez JM, Asati A, Nath S, et al. Synthesis of biocompatible dextran-coated nanoceria with pH-dependent antioxidant properties. Small. 2008;4:552–556.
[108] Karakoti AS, Singh S, Kumar A, et al. Pegylated nanoceria as radical scavenger with tunable redox chemistry. J Am Chem Soc. 2009;131:14144–14145.
[109] Lee SS, Song WS, Cho MJ, et al. Antioxidant properties of cerium oxide nanocrystals as a function of nanocrystal diameter and surface coating. ACS Nano. 2013;7:9693–9703.
[110] Raemy DO, Limbach LK, Rothen-Rutishauser B, et al. Cerium oxide nanoparticle uptake kinetics from the gas-phase into lung cells in vitro is transport limited. Eur J Pharm Biopharm. 2011;77:368–375.
[111] Patil S, Sandberg A, Heckert E, et al. Protein adsorption and cellular uptake of cerium oxide nanoparticles as a function of zeta potential. Biomaterials. 2007;28:4600–4607.
[112] Lynch I, Dawson KA. Protein–nanoparticle interactions. Nano Today. 2008;3:40–47.
[113] Kumar A, Babu S, Karakoti AS, et al. Luminescence properties of europium-doped cerium oxide nanoparticles: role of vacancy and oxidation states. Langmuir. 2009;25:10998–11007.
[114] Karakoti AS, Kuchibhatia SVNT, Babu KS, et al. Direct synthesis of nanoceria in aqueous polyhydroxyl solutions. J Phys Chem C. 2007;111:17232–17240.
[115] Kumar A, Devanathan R, Shutthanandan V, et al. Radiation-induced reduction of ceria in single and polycrystalline thin films. J Phys Chem C. 2012;116: 361–366.
[116] Vayssilov GN, Lykhach Y, Migani A, et al. Support nanostructure boosts oxygen transfer to catalytically active platinum nanoparticles. Nat Mater. 2011;10: 310–315.
[117] Singh S, Dosani T, Karakoti A, et al. A phosphate-dependent shift in redox state of cerium oxide nanoparticles and its effects on catalytic properties. Biomaterials. 2011;32:6745–6753.
[118] Pulido-Reyes G, Rodea-Palomares I, Das S, et al. Untangling the biological effects of cerium oxide nanoparticles: the role of surface valence states. Sci Rep. 2015;5:15613.
[119] Patil S, Seal S, Guo Y, et al. Role of trivalent La and Nd dopants in lattice distortion and oxygen vacancy generation in cerium oxide nanoparticles. Appl Phys Lett. 2006;88:243110.
[120] Babu S, Thanneru R, Inerbaev T, et al. Dopant-mediated oxygen vacancy tuning in ceria nanoparticles. Nanotechnology. 2009;20:085713.
[121] Shehata N, Meehan K, Hudait M, et al. Study of optical and structural characteristics of ceria nanoparticles dopes with negative and positive association lanthanide elements. J Nanomater. 2014;2014:401498.
[122] Dunnick KM, Pillai R, Pisane KL, et al. The effect of cerium oxide nanoparticle valence state on reactive oxygen species and toxicity. Biol Trace Elem Res. 2015;166:96–107.
[123] Li L, Yang HK, Moon BK, et al. Photoluminescence properties of $CeO_2$:$Eu^{3+}$ nanoparticles synthesized by a sol-gel method. J Phys Chem C. 2009;113:610–617.
[124] Vinothkumar G, Amalraj R, Babu KS. Fuel-oxidizer ratio tuned luminescence properties of combustion synthesized europium doped cerium oxide nanoparticles and its effect on antioxidant properties. Ceram Int. 2017;43:5457–5466.
[125] Shehata N, Kandas I, Samir E, et al. Parametric study of up-conversion in Er-doped ceria nanoparticles under 780 nm excitation. J Lumin. 2016;176:372–380.
[126] Woan K, Tsai YY, Sigmund W. Synthesis and characterization of luminescent cerium oxide nanoparticles. Nanomedicine. 2010;5:233–242.
[127] Kumari M, Singh SP, Chinde S, et al. Toxicity study of cerium oxide nanoparticles in human neuroblastoma cells. Int J Toxicol. 2014;33:86–97.
[128] Thai SF, Wallace KA, Jones CP, et al. Differential genomic effects of signaling pathways by two different $CeO_2$ nanoparticles in HepG2 cells. J Nanosci Nanotechnol. 2015;15:9925–9937.
[129] Peng L, He X, Zhang P, et al. Comparative pulmonary toxicity of two ceria nanoparticles with the same primary size. Int J Mol Sci. 2014;15:6072–6085.
[130] Park EJ, Choi J, Park YK, et al. Oxidative stress induced by cerium oxide nanoparticles in cultured BEAS-2B cells. Toxicology. 2008;245:90–100.
[131] Lord MS, Jung MS, Teoh WY, et al. Cellular uptake and reactive oxygen species modulation of cerium oxide nanoparticles in human monocyte cell line U937. Biomaterials. 2012;33:7915–7924.
[132] Dawson KA, Salvati A, Lynch I. Nanotoxicology: nanoparticles reconstruct lipids. Nat Nanotechnol. 2009;4:84–85.
[133] Heckman KL, DeCoteau W, Estevez A, et al. Custom cerium oxide nanoparticles protect against a free radical mediated autoimmune degenerative disease in the brain. ACS Nano. 2013;7:10582–10596.
[134] Bauer LA, Birenbaum NS, Meyer GJ. Biological applications of high aspect ratio nanoparticles. J Mater Chem. 2004;14:517–526.
[135] Wang L, Wenchao A, Zhai Y, et al. Effects of nano-$CeO_2$ with different nanocrystal morphologies on cytotoxicity in HepG2 cells. Int J Environ Res Public Health. 2015;12:10806–10819.
[136] Forest V, Leclerc L, Hochepied JF, et al. Impact of cerium oxide nanoparticles shape on their in vitro cellular toxicity. Toxicol In Vitro. 2017;38:136–141.

[137] Mahapatra C, Singh RK, Lee JH, et al. Nano-shape varied cerium oxide nanomaterials rescue human dental stem cells from oxidative insult through intracellular or extracellular actions. Acta Biomater. 2017;50:142–153.

[138] Chusuei CC, Wu C, Mallavarapu S, et al. Chemico-biological interactions cytotoxicity in the age of nano: the role of fourth period transition metal oxide nanoparticle physicochemical properties. Chem Biol Interact. 2013;206:319–326.

[139] Cheng G, Guo W, Han L, et al. Cerium oxide nanoparticles induce cytotoxicity in human hepatoma SMMC-7721 cells via oxidative stress and the activation of MAPK signaling pathways. Toxicol In Vitro. 2013;27:1082–1088.

[140] Honary S, Zahir F. Effect of zeta potential on the properties of nano-drug delivery systems – a review (Part 1). Trop J Pharm Res. 2013;12:255–264.

[141] Honary S, Zahir F. Effect of zeta potential on the properties of nano-drug delivery systems – a review (Part 2). Trop J Pharm Res. 2013;12:265–273.

[142] Frohlich E. The role of surface charge in cellular uptake and cytotoxicity of medical particles. Int J Nanomed. 2012;7:5577–5591.

[143] Vincent A, Inerbaev TM, Babu S, et al. Tuning hydrated nanoceria surfaces: experimental/theoretical investigations of ion exchange and implications in organic and inorganic interactions. Langmuir. 2010;26:7188–7198.

[144] Veriansyah B, Chun MS, Kim J. Surface-modified cerium oxide nanoparticles synthesized continuously in supercritical methanol: study of dispersion stability in ethylene glycol medium. Chem Eng J. 2011;168:1346–1351.

[145] Li K, Chen Y, Zhang W, et al. Surface interactions affect the toxicity of engineering metal oxide nanoparticles toward *Paramecium*. Chem Res Toxicol. 2012;25:1675–1681.

[146] Naganuma T, Traversa E. The effect of cerium valence states at cerium oxide nanoparticle surfaces on cell proliferation. Biomaterials. 2014;35:4441–4453.

[147] Zhou X, Wang B, Chen Y, et al. Uptake of cerium oxide nanoparticles and their influences on functions of A549 cells. J Nanosci Nanotechnol. 2013;13:204–215.

[148] Singh S, Kumar A, Karakoti A, et al. Unveiling the mechanism of uptake and sub-cellular distribution of cerium oxide nanoparticles. Mol Biosyst. 2010;6: 1813–1820.

[149] Chen S, Hou Y, Cheng G, et al. Cerium oxide nanoparticles protect endothelial cells from apoptosis induced by oxidative stress. Biol Trace Elem Res. 2013;154:156–166.

[150] Zhou X, Wang B, Jiang P, et al. Uptake of cerium oxide nanoparticles and its influence on functions of mouse leukemic monocyte macrophages. J Nanopart Res. 2015;17:28.

[151] Vassie JA, Whitelock JM, Lord MS. Endocytosis of cerium oxide nanoparticles and modulation of reactive oxygen speciesin human ovarian and colon cancer cells. Acta Biomater. 2017;50:127–141.

[152] Song MM, Song WJ, Bi H, et al. Cytotoxicity and cellular uptake of iron nanowires. Biomaterials. 2010;31:1509–1517.

[153] Felix LP, Perez JE, Contreras MF, et al. Cytotoxic effects of nickel nanowires in human fibroblasts. Toxicol Rep. 2016;3:373–380.

[154] Xie X, Aalipour A, Gupta SV, et al. Determining the time window for dynamic nanowire cell penetration processes. ACS Nano. 2015;9:11667–11677.

[155] Szymanski CJ, Munusamy P, Mihai C, et al. Shifts in oxidation states of cerium oxide nanoparticles detected inside intact hydrated cells and organelles. Biomaterials. 2015;62:147–154.

[156] Zhang Q, Ge K, Duan J, et al. Cerium oxide nanoparticles protect primary mouse bone marrow stromal cells from apoptosis induced by oxidative stress. J Nanopart Res. 2014;16:2687.

[157] Babu KS, Anandkumar M, Tsai TY, et al. Cytotoxicity and antibacterial activity of gold-supported cerium oxide nanoparticles. Int J Nanomedicine. 2014;9: 5515–5531.

[158] Peters R. Xenopus protocols. New York: Springer; 2006. p. 235–258.

[159] Ting SRS, Whitelock JM, Tomic R, et al. Cellular uptake and activity of heparin functionalized cerium oxide nanoparticles in monocytes. Biomaterials. 2013;34:4377–4386.

[160] Lord MS, Tsoi B, Gunawan C, et al. Anti-angiogenic activity of heparin functionalized cerium oxide nanoparticles. Biomaterials. 2013;34:8808–8818.

[161] Lord MS, Farrugia BL, Yan CMY, et al. Hyaluronan coated cerium oxide nanoparticles modulate CD44 and reactive oxygen species expression in human fibroblasts. J Biomed Mater Res A. 2016;104A: 1736–1746.

[162] Xu C, Lin Y, Wang J, et al. Nanoceria-triggered synergistic drug release based on $CeO_2$-capped mesporous silica host-guest interactions and switchable enzymatic activity and cellular effects of $CeO_2$. Adv Healthcare Mater. 2013;2:1591–1599.

[163] Weaver JD, Stabler CL. Antioxidant cerium oxide nanoparticle hydrogels for cellular encapsulation. Acta Biomater. 2015;16:136–144.

[164] Qiu Y, Rojas E, Murray RA, et al. Cell uptake, intracellular distribution, fate and reactive oxygen species generation of polymer brush engineered CeO2-x NPs. Nanoscale. 2015;7:6588–6598.

[165] Song W, Lee SS, Savini M, et al. Ceria nanoparticles stabilized by organic surface coatings activate the lysosome-autophagy system and enhance autophagic clearance. ACS Nano. 2014;8:10328–10342.